



Thermal analysis for improvement of mechanical properties in fused filament fabricated parts

Md Aftab Alam¹ · Krishnanand¹ · Abhishek Patel¹ · Rajesh Purohit¹ · Mohammad Taufik¹

Received: 6 April 2022 / Accepted: 1 July 2022 / Published online: 28 July 2022
© The Author(s), under exclusive licence to Springer-Verlag France SAS, part of Springer Nature 2022

Abstract

Additive manufacturing techniques are widely used in the present manufacturing era because of their ability to manufacture intricate products. Fused filament fabrication (FFF) is one of the most commonly adopted additive manufacturing technology, which involves the extrusion of the semi-solid polymer through the nozzle to be deposited in layers to form the part. In FFF, the polymer melt being deposited, forms the bonds with the neighboring pre-deposited melt during the part fabrication. The pre-deposited melt is at the low temperature compared to the polymer melt extruding out of the nozzle; hence the heat transfer occurs due to temperature gradient by the mode of conduction and convection. The commercialization of the FFF technology in a wide range of industrial applications still seems to be constrained due to several drawbacks such as insufficient mechanical properties, poor surface quality, and low dimensional accuracy. The grade of FFF-produced products is affected by various process parameters, for example, layer thickness, build orientation, raster width, or print speed. In FFF, process parameters are optimized to improve the quality of the final printed part. The cost of post-processing is also reduced as a result of parameter optimization. In this study, the influence of the convection coefficient on bond formation was investigated, and a model for predicting bond size in terms of convection coefficient is discussed for a given set of parameters. This work also aims to study the effects of thermal properties on neck formation and the effects of neck formation on strength, surface finish, and dimensional accuracy of the printed parts. In addition, this study reveals the problems and difficulties found in previous works, potential future scope in this area has been analyzed, and new research approaches are suggested.

Keywords Additive manufacturing · AM · Material extrusion · ME · 3D printing · Fused deposition modeling FDM · AM · Thermal analysis · TA · Bond formation · Convection heat transfer coefficient · Stereolithographic · SL · Pre-heating deposition · Neck growth · Dimensional accuracy · DA · Process parameter · Part characteristics

1 Introduction

Additive manufacturing (AM) technology is used to produce 3D objects directly from the part models made on computer by depositing material on layer over layer fashion [1, 2] It allows for designing a wide range of prototypes and operational parts with complex shapes and geometry, including all those produced using a topology optimization technique [3, 4]. Any additive manufacturing process generally consisted of four steps, and a sequence of these steps is followed to fabricate the physical part from a virtual 3D CAD model.

3D modelling of the part using the computer is very first step for AM process. This solid CAD model is then converted into STL file format, and transported to an AM process planning software. In the second step, STL file is imported to process planning software for slicing and g-code generation [5–7]. Slicing tools such as Cura, KISSlicer, Slic3r, etc. are used to slice the STL file [8]. Before slicing; position, orientation, support requirement and various other process parameters are decided and then slicing process is performed, which results in the tool path (G-Code) generation. In the third stage the generated G-code is the transported to the additive manufacturing system to fabricate the actual part. Support removal, improving surface finish, etc. are some operations which are performed in the fourth stage of AM process. The fused filament fabrication (FFF) is one of the popular AM technologies. In the FFF process, a continuous wire of a solid thermoplastic (i.e., Acrylonitrile Butadiene

✉ Mohammad Taufik
taufikmohd86@gmail.com

¹ Department of Mechanical Engineering, Maulana Azad National Institute of Technology (MANIT), Bhopal 462003, India

Styrene (ABS), Polylactic Acid (PLA), Polycarbonate (PC), Polysulfone, etc.) is used as feed material, that is known as filament. In FFF process, the G-Code file generated in the second stage, is utilized to define tool motion for layer-by-layer deposition of heated filament on a build surface. One of the most severe drawbacks of 3D printing technology, particularly for FFF-made objects, is poor surface quality. The stepping effect is the built-in feature of the parts made through FFF technology; hence rough surface could not be eliminated. However, researchers are consistently attempting to reduce it. There will essentially be two approaches for improving surface smoothness in post processing. Surface smoothing can be accomplished chemically or mechanically. Researchers found a new way to efficiently minimize the surface roughness of FFF printed parts by employing a laser-based beam based post-processing technique [9, 10]. Over the last three decades, various additive manufacturing processes based on powder, solid, and liquid materials have been developed. Stereo lithography (STL) of a photopolymer liquid, Fused Deposition Modelling (FDM) with thermoplastic polymer material, fused filament fabrication (FFF) with wire filament, Laminated Object Manufacturing with plastic laminations, and Selective Laser Sintering with plastic or metal powders are some examples of AM applications. 3D printing is an additive manufacturing process classified according to the feed material utilized. Solid, liquid, and powdered feed materials are the three categories of feed materials [11]. Fused Deposition Modelling (FDM) is one of the most extensively utilized solid-materials-based additive manufacturing techniques. Because of its design flexibility, lack of scrap, low process cost, and strong mechanical qualities. Therefore, compared to liquid and powder material type techniques like Stereo Lithography (SL) and Selective Laser Sintering, the created products have a relatively low surface roughness (SLS). Cost, design freedom, build time, waste generation, and the energy consumption is significant advantages of additive manufacturing over traditional manufacturing. Compared to traditional production, the AM technique saves money on post-processing [12]. AM technology provide unrivaled design flexibility and complexity compared to secondary machining processes. Forging, joining, and installation costs are often minimized in additive manufacturing. 3D printing is significantly more enticing than traditional machining processes since it allows greater design flexibility. While AM has some benefits over conventional manufacturing technologies, it also has several disadvantages, including staircase effects, surface roughness, and dimensional accuracy. Most researchers experimented with various post-processing procedures to overcome the restrictions [13]. The impact of the SLS process on the energy consumption of AM technologies has been investigated. It was discovered that there is even a slight difference in

energy usage between different materials when implementing AM techniques. However, when standard manufacturing techniques are utilized, the difference is noticeable. AM-produced parts conserve energy while in operation because they are compact and lightweight, which is useful in the automotive, medical, and aerospace industries and for producing functional parts and engineering prototypes. AM technology is presently used in many industries, including research, engineering, medical, the military, construction, architecture, fashion, education, and the computer industry. Additive manufacturing advantages to traditional manufacturing in cost, design flexibility, time to build the part, waste generation, and energy utilization [14, 15]. In the conventional manufacturing process, external support elements are required. As a result, it uses more energy than the additive manufacturing technique [4]. Material extrusion is fundamental to 3D printing. 3D printing techniques have gained popularity due to their ease of use, low cost, and environmental responsibility. There is no waste, and the 3D printing procedures are nontoxic, odorless, and inexpensive. S. Scott Crump established fused deposition modeling (FDM) in the late 1980s, and Stratasys put the technology into practice in 1990. As a result, such a patent expired in 2009. Such printing methods are used without paying Stratasys for authorization [16, 17]. This 3D printer became available after a big open-source development community created commercial versions. As a result, the cost of FDM technology has dropped by two orders of magnitude since its launch. Fused filament fabrication (FFF) is fused filament manufacturing [18, 19]. Fused deposition modeling (abbreviated as FDM) or filament freeform fabrication is also known as fused deposition modeling. It's a 3D printing process that employs a thermoplastic filament continuously fed into the printer. Three-dimensional (3D) printing is accomplished by feeding a coil of wire into an extruder machine using a roller mechanism. To melt the filaments in the extruder at a high temperature. Extruded filaments are ejected from the nozzle and deposited layer-by-layer on the build plate, following a predetermined route. In the material extrusion process based on 3D printing technology, materials like filaments and pellets are commonly employed. FDM technique has several advantages over 3D printing, including flexible design, low purchase and maintenance costs, a large range of commercially available materials, fast changeable materials, nontoxic materials, portable platforms, and low-temperature operation. As a result of these advantages, FDM has grown in popularity as a well-suited technology for micro engineering, is constantly improving, and has transcended the limited capabilities for micro component creation that defined this technology only a few decades ago [20–22]. Fused deposition modeling (FDM) is currently used in a wide range of industrial applications such as automobiles, aerospace and electronics, pharmaceuticals, medical and consumer goods, sculpture, and jewelry design [16, 23]. The FDM process uses

the semi-liquid filament's heat energy to build a link between two consecutive filaments. The bond strength between the filaments and FDM parts is a significant factor in estimating the integrity and characteristics of the parts [17]. The main objective of this paper is to explore the bonding and mechanical properties, as well as neck growth and surface roughness, between the materials used in the FDM technique, such as ABS and PLA, as the filament material [2, 24, 25]. Knowing the bond formation is critical in determining the component's strength in the literature review. So little work has been reported in the literature on a quantitative analysis of heat transfer, which is essential for the strength of the bond produced in the FDM process [26, 27]. As a result, it's essential to consider the properties of the formed bond and assess the dynamics of bond creation, also referred to as neck growth. The influence of the convective heat transfer coefficient on the neck growth process in FDM has been investigated in this paper. In this study, the bonding quality is determined by the degree of moisture or the neck size formed between neighboring filaments. The goals of this research are to model the dynamics of bond formation along polymer filaments during the FDM extrusion process and to investigate the impact of various manufacturing process parameters such as air gap, build orientation, extrusion temperature, infill density, infill pattern, layer thickness, printing speed, raster width and raster orientation on bond formation as well as mechanical characteristics [28, 29]. This study can also help present and future scholars, practitioners, and the general public establish FDM experiments and conduct research on enhancing or maximizing the features of FDM products.

1.1 Materials for filament

Material used as filament should have a minimum rigidity to withstand the pushing force exerted by the extruder, so that solid part of filament could act as plunger for the melted part. In fused filament fabrication process, generally thermoplastic materials are used as a filament. In this section most commonly used filament materials have been discussed.

1.1.1 Acrylonitrile butadiene styrene

The thermoplastic polymer and amorphous ABS materials are generally used in 3D printing or FDM. Thermoplastic material was initially produced by the three different monomers known as ABS. The monomers of ABS are abbreviated such Acrylonitrile, Butadiene, and Styrene. ABS has divided into two-phase polymer systems [28]. A rubber particle butadiene copolymer produced it with a group of copolymers called styrene-acrylonitrile (SAN). This material is trendy and widely used worldwide—the closeness of the SAN. The rubber content in the fraction of ABS is 10–25% used commercially. The Percentage of polyvinyl

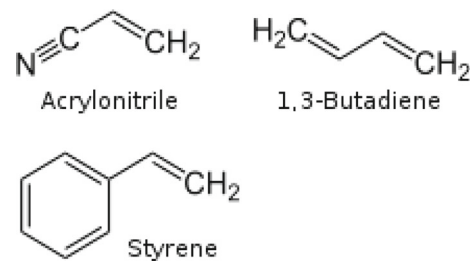


Fig. 1 Monomers of ABS polymers

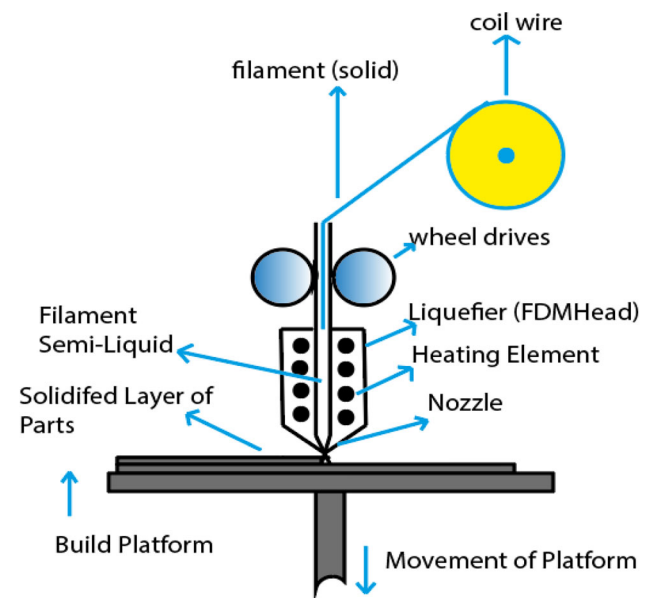


Fig. 2 Schematic of material extrusion (ME) process

chloride is used at 45% for blending. The polyvinyl chloride percentage is significantly higher, and it has valuable for better properties. ABS has the most significant consumption rate compared to other thermoplastic materials. The manufacturing and chemistry of ABS are in two-phase. The first phase is the regular styrene-acrylonitrile (SAN) phase and a scattering phase of implanted polybutadiene copolymers. Each phase plays a role necessary for a material characteristic of ABS. The monomers of ABS polymers as shown in Figs. 1, 2.

The composition of ABS is acrylonitrile 21–27%, butadiene 12–25%, and styrene 54–63%. Initially, acrylonitrile supported chemically and balanced heat. Butadiene monomers provide higher strength and toughness impact on polymer materials. The styrene monomers have desirable rigidity. SAN has copolymer but has additional characteristics such as chemical resistance, surface finish, hardness, and improved toughness. The thermal property of ABS material mainly depends on the glass transition temperature. When the temperature rises, ABS material achieves desirable toughness and ductility and reduces tensile strength while elasticity

decreases in tension. The main challenge is to improve the tensile strength of ABS material [12]. It has toughness and impact resistance of two significant mechanical properties [30]. ABS has a 230 °C-melting point higher than polylactic acid (PLA). ABS is not, but PLA is biodegradable. ABS has a low risk of jamming nozzle [24, 31].

1.1.2 Poly lactic acid (PLA)

PLA thermos-plastic formula is $(C_3H_4O_2)_n$. It is produced from renewable resources and is very economical. It is the second-highest consumable material. PLA has by the use of condensation of lactic acid monomers. For preparation, it required less than 200 °C [32]. In the FDM process, PLA is used as a polymer of thermoplastic material [33]. It increases biodegradable thermoplastic for prototype process and functional parts with good quality [34]. PLA requires less energy and temperature and does not require a heated bed [35]. Demerits are the jamming of the nozzle during parts printing. Compared to ABS, it has higher tensile strength, low bending, and ductility [30, 36]. PLA printed parts require extra care compared to ABS [37].

1.1.3 Polycarbonates (PCs)

Polycarbonates are one type of thermoplastics distinguished for outstanding strength, hardness, and durability, and several of them are translucent. It has to be high-temperature thermoplastics with excellent heat resistance, layer-to-layer solid contact, and a high-quality surface.

1.1.4 Polyether ether ketone (PEEK)

Polyether ether ketone is a good choice since it is a thermoplastic with excellent heat resistance, mechanical qualities, and chemical stability. Especially compared to PLA or ABS, it offers better mechanical characteristics. It is a biomaterial, and it is deemed a potential bone healing polymer that can be used in human prosthetics.

1.1.5 Polyetherimide (PEI)

The transportation sector favors polyetherimide because of its excellent strength-to-weight ratio, low smoke generation, and low smoke toxicity. While printing required a high extrusion temperature and bed temperature, ULTEM™ 9085 is the company's trademark. Because of its lesser density and toxicity characteristics, it is suitable for usage in aircraft cabins.

1.1.6 Nylon

Nylon is a good option if the need to produce highly flexible and durable components. It possesses a high level of toughness and impact resistance. However, it is hugely moisture reactive, and nylon has a similar warping ability to ABS. Nylon, along with many other FDM filaments, is hygroscopic, which means it absorbs moisture from the atmosphere when exposed to it. Moisture absorption degrades filament characteristics, which leads to component deterioration.

1.1.7 Other materials

In addition to the materials stated above, several others can be implemented. Various materials aren't typically utilized or studied as filaments. Some examples appear to include high-impact polystyrenes (HIPs), polyphenylsulfone (PPSF), polyethylene terephthalate glycol-modified (PETG), thermoplastic polyurethane (TPU), bio-composite filaments, ceramic filaments, and other composite material filaments. The majority of these materials are currently in development or challenging to get on the marketplace. Section 4 later describes the properties of thermoplastic filaments material with tables. Section 2 introduced the equipment along with the extruder unit's material extrusion.

1.2 Material extrusion of extruder unit in fused filament fabrication (FFF) process

The fused deposition modeling (FDM) technique is performed in the extrusion process and is indicated in schematic diagram 2. In the material extrusion process, thermoplastic filament material is fed into the extruder unit to melt [38] by then heated at maximum liquefier temperature. The extruded filament is supplied through the nozzle to the deposition surface to produce parts [39].

To analyze the material extrusion process using the FDM system, set the experimental parameters for requirements such as estimated filament feed rate, liquefier temperature, and velocity of the nozzle head. In the fused deposition modeling (FDM) process, acquire the optimum heat input at the extruder unit [40, 41]. Section 3 discusses preheating a construction plate that already exists in the material extrusion process.

1.3 Preheating on existing build plate surface

The bond between two adjacent filaments and the building plate. It is found in this literature survey, a lack of thermal energy on the surface. Because of this reason, a reduction in thermal properties and neck growth appeared [17]. Some processes are applied to preheating various light sources, including infrared and laser light [20], and require preheating

across the existing surface with hot air during the extrusion process. The Source of light supplies thermal energy for pre-heating when traveling from the extrusion head of the nozzle on the build surface to the top side of the build surface [8]. When melted filament material comes into contact with the existing build plate [8]. When the two filaments contact each other to form a bond, the bond takes place by the touch of wetted filament, inter-molecular diffusion, and randomization process required for the powerful intermolecular make a hole in glue take place to a more significant limitation compared to deposition of filament without heat transfer [42]. With preheating the surface, change the characteristics of bond strength and mechanical properties are enhanced by more than 50%. And as the printing speed increases, so does the preheating. The surface effect of a heated region when put in to achieve better adhesion and avoid warping of final part [2].

1.4 Thermal analysis considering diffusion in the fused deposition modelling (FDM) process

Process parameters and significance of thermal analysis in fused deposition modeling (FDM) process. Such as thermal conductivity (k), heat capacitance (C), density (ρ), viscosity (μ), and these parameters have physical significance to the improvement of bond formation quality [1]. Since the bonding of thermoplastic polymer components in the material is thermally operated, the temperature of the interfaces has been used to estimate the bond's quality level and better strength characteristics of mechanical parts [43]. The formation of bonds in fused deposition modeling (FDM) depends on the thermal properties, liquefier, envelope temperature, and temperature cooling profile. Heat transfer occurs due to the temperature gradient (ΔT), and the transfer of heat is a function of temperature and the liquefier's thermos-physical properties, tip modeling, and material, as well as the filament's cross-sectional size and volume flow rate. Generally, the liquefier temperature (TL) of thermoplastic material ABS P004 is 270 °C, and the ambient temperature is 70 °C [1]. The thermoplastic semi-molten material is deposited, and the semi-molten filament is junctions with environmental material. The interface temperature must be higher than the glass transition temperature of 94 °C. For the adhesive bond to develop quickly [44]. If the interface temperature is below the glass transition temperature, no reaction occurs between the deposited filaments with surrounding material and no bond formation [18]. The filament's temperatures are slowly decreasing to cool at the ambient temperature. The process of cooling has transient as well as substantially complex nature-wise. The physical significance of the short model for the cooling process is time is increases with decreasing temperature [19]. The model of the cooling process in a transient state is derived in Sect. 6, and steady-state heat transfer analysis is

Table 1 Thermal properties of ABS P400 [1] and PLA [45]

Parameters	Values	
	ABS	PLA
Thermal conductivity $k, \frac{W}{mK}$	0.177	0.13
Specific heat $C, J/kg \cdot K$	2080	1800
Density $\rho, kg/m^3$	1050	1240
Glass transition temperature $T_g, ^\circ C$	110–120	60–65
Thermal diffusivity $\alpha, mm^2/s$	0.12	0.058

Table 2 Thermal properties of poly-ether ether ketone (PEEK) [26]

Property	Value
Melting temperature (T_m)	343°C
Glass transition Temperature (T_g)	143°C
Density (ρ)	1320kg/m ³
Thermal conductivity coefficient (k)	0.25W/m°C
Specific Heat Capacity (C)	2177J/Kg°C

performed to get heat input into the extruder unit explained in Sect. 5 (Tables 1, 2).

1.5 Heat input for melting of filament in fused deposition modelling (FDM) process

Considering steady-state heat transfer analysis is performed in the FDM system. To get heat input Q_{in} at extruder unit because melting thermoplastic filament in the material extrusion process [46] is expressed in Eq. (6). The existence of a temperature difference is a requirement for heat transfer rate. When thermal energy is transferred, an applied force is needed to handle temperature differences—the net amount of heat transfer Q_{in} throughout in time interval to calculated from the Eq. (1).

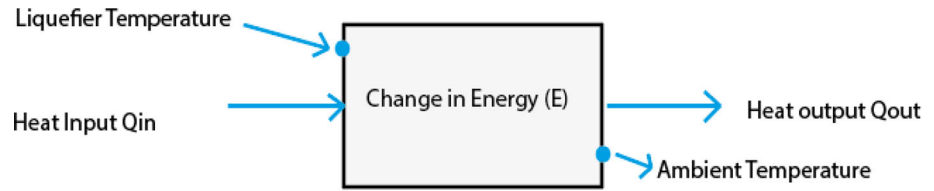
$$Q = \int_0^{\Delta t} Q * dt (KJ) \quad (1)$$

Heat flux is the heat transfer rate per unit cross sectional area. It is expressed in Eq. (2).

$$q* = \frac{Q*}{A} w/m^2 \quad (2)$$

It was noted that energy interaction by the rate of heat transfer by balancing the energy equation in extruder unit [47] is expressed in Fig. 3. Consider a steady state conduction through extruder unit and temperature difference across the

Fig. 3 Schematic of heat input of extruder



unit is $\Delta T = (TL-TE)$

$$Q_{in} - Q_{out} = \frac{dE}{dt} \tag{3}$$

where (Q_{in}) heat input at liquefier temperature and (Q_{out}) heat rejected at surrounding temperature.

For steady-state operation:

$$Q_{in} = Q_{out} = Constant \tag{4}$$

$$Q_{in} = m.Cp.(TL - T\infty) = \rho.V.Cp(TL - T\infty) \tag{5}$$

where C is specific heat is to be defined by the amount of thermal energy required to increase temperature unity mass of gas by unity temperature.

$$m = \rho V \text{ and } A = \frac{\pi}{4}d^2$$

Putting the value of m and A in equation (5) to get the final expression in terms of Q_{in} heat input as below.

$$Q_{in} = \pi\rho d^2 Vf Cp(Tl - T\infty)/4 \tag{6}$$

where A, ρ, d, Cp, Vf, Tl and $T\infty$ are the cross-section area of filament, density of filament, diameter of filament, specific heat of filament at room temperature, liquefier temperature and room temperature at 20 °C [40].

1.6 Cooling process of extruded filament in (FDM) process

The cooling process of extruded filament is modelled by using an analysis application. An assumption of lumped capacity should be considered during the analysis. Assume a homogeneous temperature circulation all over the cross-section, and temperature variation in the cross-section area ignored. The idealized filament cross-section is used as the circle in Fig. 4a and b in the cooling process, consider a one-dimensional 1D transient heat transport model. For the purpose of determining a single elemental filament [1, 18, 44].

1. Considering the assumption for simplification and the thermoplastic material melting in the extruder of nozzle

takes, the cross-section is circular, which is assumed to be cylindrical.

2. Depositing the cylindrical filament on the platform. Assume the semi-infinite length. Assume that sinks into the build platform.
3. For simplification of the one-dimensional heat transfer model assumed that the uniform temperature distribution on the entire cylindrical roads.
4. Deposition of the filament on the build platform by extruder unit with a constant rate.
5. The tip of the nozzle is mounted on the bottom part of the extruder head. Selecting the prior nozzle time over the origin coordinate system to formulate

$$\text{Energy in from left side of the surface } Q_{in} = -KA \frac{\partial T}{\partial x} x \tag{7}$$

$$\text{Energy out from the right side of the surface } Q_{out} = -KA \frac{\partial T}{\partial x} |x + dx \tag{8}$$

$$\text{Change in internal energy} = \rho CA \frac{\partial T}{\partial t} dx \tag{9}$$

$$\text{Convection heat transfer with air} = h1.(P - A).(TL - TE)dx \tag{10}$$

$$\text{Convection heat transfer with foundation} = h2.A.(TL - TE)dx \tag{11}$$

where P and A , perimeter and area of the shape. Mass of foundation is much higher than filament mass so that the conduction at the interface does not much change the foundation temperature. Conduction heat transfer of foundation considers in the form of convection. For the differential element, the energy balance is

$$\rho CA \frac{\partial T}{\partial t} = \frac{A(k \frac{\partial T}{\partial x})}{\partial x} - hP(TL - TE) \tag{12}$$

where $h = h1 + h2$, with range estimated from 50 to 100 W/m² °C. The h covers the total heat transfer coefficient effect of both convections with air and conduction with foundation.

Boundary condition:

$$\text{with } T = T0, \text{ at } x = 0 \text{ and } t \geq 0 \tag{13}$$

$$\text{And } T = T\infty, \text{ at } x = \infty \text{ and } t \geq 0 \tag{14}$$

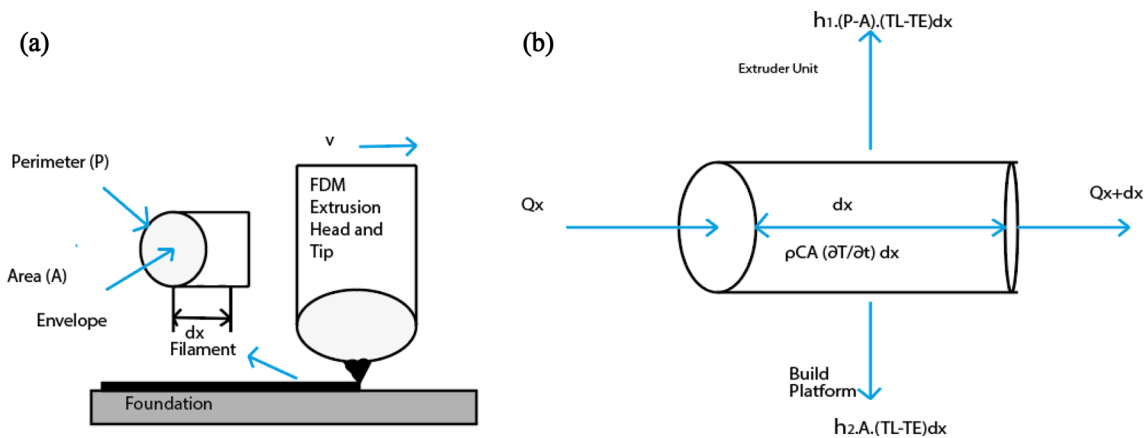


Fig. 4 Schematic of (a) deposition and (b) cooling of a filament in FDM

The velocity of nozzle head moves at a constant velocity v along the X-axis when extruding. $x = vt$ And the time dependence is $\partial T/\partial t$ is transformed to:

$$\frac{\partial T}{\partial t} = \frac{\partial T}{\partial x} \frac{\partial x}{\partial t} = \frac{\partial T}{\partial t} v \tag{15}$$

The governing equation reduces to an ordinary differential equation form:

$$\rho C A v \frac{\partial T}{\partial x} = \frac{A(k \frac{\partial T}{\partial x})}{\partial x} - h P (T L - T E) \tag{16}$$

Applying the boundary condition (13) and (14) into Eq. (16) to get the analytical solution in terms of temperature distribution profile.

$$T = T E + (T L - T E) e^{-m x} \tag{17}$$

where T is the average or interface ($T_{avg.}$) continuously varying with time and hence interface temperature described as the function of time (t).

In transient heat conduction, heat transfer due to conduction vary with time.

With $m = \frac{(\sqrt{1 + 4\alpha\beta}) - 1}{2\alpha}$ and $x = vt$

$$\text{where } \alpha = \frac{k}{\rho C v}, \text{ and } \beta = \frac{h P}{\rho C A v} \tag{18}$$

where the term m is the coefficient constant of α and β are roots, the value of m written in the form of quadratic equation [19, 44].

$A =$ Area of cross section

$P =$ Perimeter of cross section

$v =$ Velocity of extrusion head

And thermal properties are ρ, k, c

Putting the value of $x = vt$ in equation (17) to modified in the terms of m

$$T = T E + (T L - T E) e^{-m v t} \tag{19}$$

Therefore, $m = \frac{1}{v t} \ln \frac{(T L - T \infty)}{(T - T \infty)}$ (20)

Putting the values in Eq. (18), and β is expressed in terms of m and α , its result in equation (21)

$$\beta = m(m\alpha + 1) \tag{21}$$

In order to determine the convection coefficients' relationship, (h) and time (t), when put the value of m from Eq. (20) and along with the value of β from (18) into Eq. (21) and resulting in Eq. (22).

$$h = \frac{(\rho A C v)}{P} \left(\frac{1}{v t} \ln \frac{(T L - T \infty)}{(T - T \infty)} \right) \left(\frac{\alpha}{v t} \ln \frac{(T L - T \infty)}{(T - T \infty)} \right) + 1 \tag{22}$$

From Eq. (22), analyse that the controlling parameters are the velocity of nozzle head, extruder unit temperature, surrounding temperature and thermal properties of the material, etc. The natural or free convection occurs between the extruded filaments with atmospheric air, and its atmosphere plays a vital role in cooling extruded filaments [19]. A hand data book of heat transfer is used as a reference in thermal analysis of fused filaments fabrication process [47]. The thermal study developed in the FFF process described in Sect. 7

predicts the bond formation and neck growth and neck formation's effect on parts strength, surface finish, and part accuracy.

2 Discussion

2.1 Prediction on bond formation

When forming a bond between two filament materials in fused deposition modelling (FDM). The bond formation occurs through three processes 1. Wetting 2. Diffusion at interface 3. Randomization. The first step at interface intermolecular surface touching by wetting. The molecule undergoes motion in the preferred configuration to attain equilibrium. The diffusion of molecules at the entire surface of the existing plate at the interface and reaction to developing the initial bond formation occurs chemically over the interface. After that, the randomization process extended for molecular diffusion of bond parts to undergo critical states [1]. Increasing the liquefier temperature so there are no significant effects on deposition filament and achieve the considerable strength of the bond between the adjacent materials [18]. In the FDM process, the temperature of deposition material must be greater than the transition temperature, somewhat extended over a specific period. In this state, diffusion of molecules takes place on the interfaces. The interface between the filaments slowly disappears and grows the quality of bond and mechanical property at the interface [19, 24]. In the literature survey, it has been found that the formation of neck size stops well before the glass transition temperature. It decreases the interface temperature from extrusion temperature to surrounding temperature. It considers the convection heat transfer coefficient varying from 50 to 100 W/(m² k). Interface temperature exponentially decreases with time. The main reason is that the significant thermal gradient between the interfaces and surrounding results in a higher rate of convection heat transfer due to an increase in the higher rate of heat transfer at a later stage interface, and surrounding temperature decreases. It was found that the cooling profile for convection heat transfer coefficient. If changing the coefficient value, a new cooling profile is generated. That means it depends entire limiting sintering temperature over the convection heat transfer coefficient [17].

2.2 Prediction on neck formation

The neck growth observation between the filaments in the fused deposition modelling and polymer sintering model is combined with heat transfer [48]. The neck growth is dependent on the temperature of material properties such as density, thermal conductivity, heat capacitance, viscosity, and surface

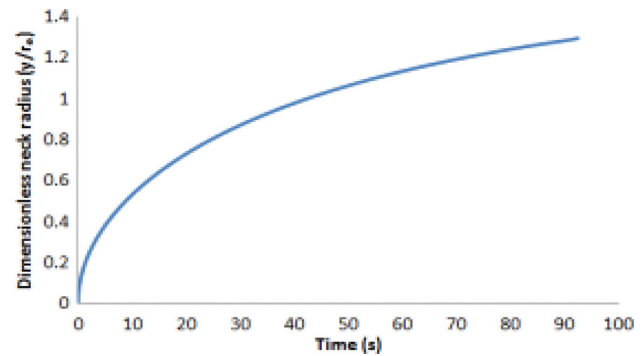


Fig. 5 Variation in dimensionless neck radius with time [19]

ension. The neck formation is found in the analysis of experimental data [17]. The literature survey observed that in parts produced in the fused deposition modelling (FDM) process, the bottom layers of elements show higher neck growth than the layer at the top. Formation of neck growth occurs due to conduction heat transfer to another filament layer deposited above the bottom layers, and a hence higher temperature is maintained at the bottom layers of parts for the more extended time shown in the below graph Fig. 5 [19]. The literature found that the bond strength and mechanical properties [49] of the FDM process formed parts depend on the dimensional neck size. It is essential to achieve the desired dimension of neck size [2]. The highly dependent parameters belong to the thermal properties of the thermoplastic polymer material [50]. The effective velocity of the nozzle head, the diameter of filament, extrusion temperature, ambient temperature, and convection coefficient condition improve the neck growth between the materials in the 3D printing process [44, 51]. And it is seen that during the survey, extrusion temperature has a significant role in forming the quality of bond compared to the surrounding temperature.

Effect of temperature and convection coefficient on dimensional neck size. It found that dimensionless neck growth increases correspondingly with time. The bond formation between the neighbouring layer of the thermoplastic polymer process is (1) surface contact by wetting. (2) Neck size formation. (3) Inter-diffusion of the molecule at the interface surface (4) Randomization. In Fig. 5. Shows the neck growth steps infused diffusion modelling process. The bonds between the two neighbouring layers involve surface touching, dimension of the size of the neck growth, and attraction of molecule, as shown in Fig. 6. The bond takes place between the next filament in a layer. The layer formed between the extruded filament in a row and observed that bond formation occurred. The solidification of filament attains less time to cool the filament, and due to this get, partial neck formation between the filaments results in induced porosity in the layer [34]. Increasing the porosity reduces parts strength in the fused deposition modelling (FDM) process [17].

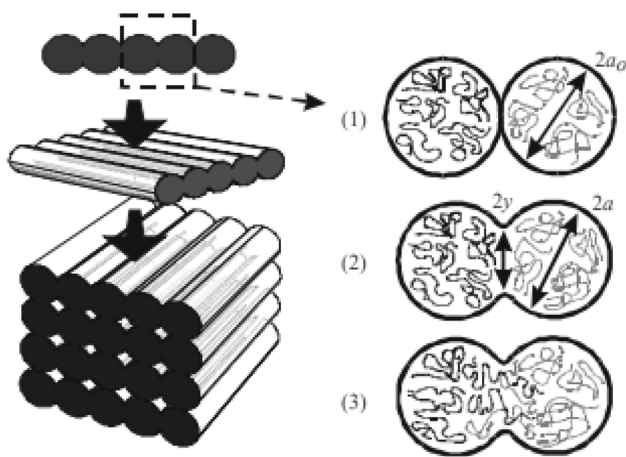


Fig. 6 Neck growth in FDM [17]

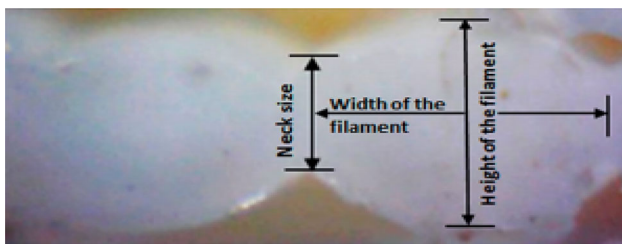


Fig. 7 Neck dimension, height and width of filament [61]

2.2.1 Effect of neck formation on part strength

When the filament is extruded on the deposition surface to produce parts in a three-dimensional (3D printing) process, the bond formed by an deposited road is essential [52]. The bond developed between two adjacent road is known as neck formation or neck growth. The dimension of neck size is used to predict the bond strength quality. The surface tension of thermoplastic polymer material influences the growth of neck size, and heat is then transferred to the environment [1]. Use an image processing tool; the size of the dimensionless neck is measured. The literature observes that the surface tension of nanocomposite is higher than ABS polymer [53, 54]. The nanocomposite was observed the more elevated surface tension that is useful to form better neck size between the two filaments shown in the [55, 56] Fig. 7—and resulting in the enhancement to FDM of the strength of parts. Observed that a significant neck dimension would tend to the reduction of the void between the two neighbouring filaments [57]. In general, the porosity of nanocomposite is lesser than the ABS polymer. More secondary, the porosity leads to the bond of parts strength [54, 58].

In the analysis of tensile properties such as tensile strength, yield strength, modulus, and elongation observed at different nanocomposite compositions, the effect of nanocomposite on the tensile properties of the filament [14]. When the increased

percentage composition of nanocomposite is 5–10% with improved tensile and yield strength properties, gradually growing, and the percentage of nanocomposite by 15% drop the strength properties.

The maximum parts strength was observed at 10% of nanocomposite and minimum at 15%, respectively, as shown in Figs. 8a and b. The result of neck growth to the enhancement of ultimate tensile and reduction in shrinking [59, 60] Figs. 9a, b, and 10.

The neck growth rate is significant because of the existence of heat up to a suitable time has done for expiring and beyond the specific range of time to the reduction in neck growth rate and ultimately reached to the closing value. Dimensional neck in a significant role in the FDM process to estimate the Tensile strength [62]. Tensile load is the function of time. The neck dimension's growth rate reached proportion before the filament fully solidified. As resulting the value of tensile strength increased [63]. In the FDM process, the extrusion head deposits the material one layer over another to maximize the time to increase the temperature needed to grow the neck size greater and enhance the strength of the part. The ultimate tensile load test by the ASTM-D638 simple tension test in the FDM process. It was observed from the data strength of the 3D printing component in the transverse direction is higher over the build direction due to the stability of the interlayer checking layout being higher than that of the interlayer examining layout [64]. The thermal energy of the semi-molten filament is used to bond the two filaments simultaneously. The strength of parts depends on the interlayer and inter-layer bonding [65]. The strength of bonding is different due to different temperature gradients. Bond strength is characterized by the rate at which the neck among the raster grows, as shown in Fig. 11. The quality of bond strength is determined by the growth of the neck dimension between two neighbouring polymer materials, which causes diffusion, crosslinking, and neck growth enhancement is possible at the interface and improvement in parts strength [66]. The fracture variation takes place between the intra-layer and interlayer [67].

The test specimen is prepared alternately in the direction of extrusion. The tension test of the specimen by UTM to validate the bond strength is dependent on the raster orientation and neck formation is shown in Fig. 12.

It is very significant to examine the mechanical characteristics of FDM parts among the filament to produce the bond quality. The dimensional size of neck formation and high rate of wetting formed between the two filaments is practical to Estimate the bond quality. Some process parameters affect the mechanical properties and developed porosity, such as the air gap between the filament and the raster's width [69]—the investigation of porosity in 3D to poorer bond quality. Hence lower the porosity, the better the mechanical properties [70]. Porosity affects the intra-layer and inter-layer bonds. The

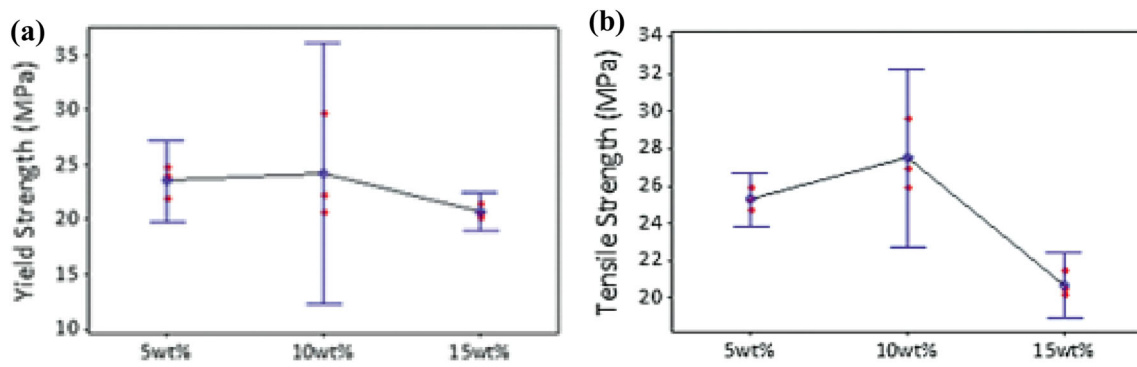


Fig. 8 (a) Yield strength vs Nanocomposite percentage, (b) Tensile strength vs Nanocomposite percentage [61]

Fig. 9 (a) surface contact
(b) necking [3]

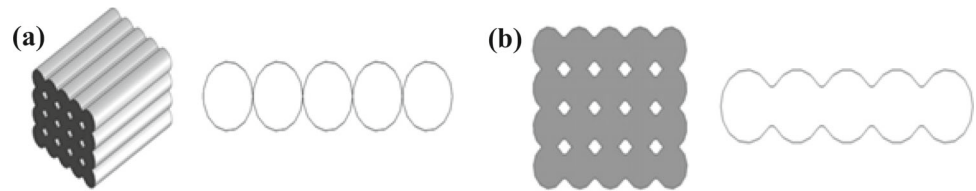
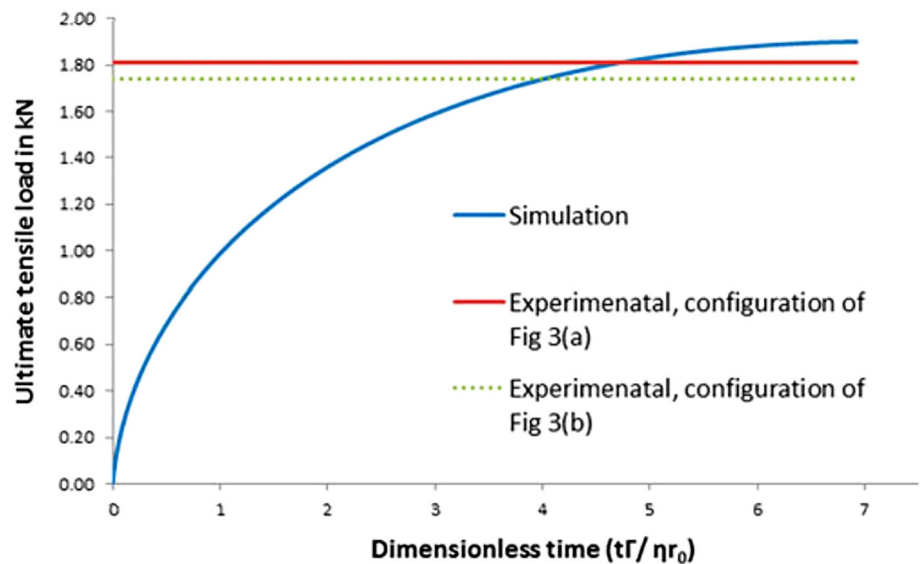


Fig. 10 Ultimate tensile load vs Dimensionless time [3]



voids are formed due to improper deposition. When deposition strategy [71] is well under control, so more minor porosity forms, and inter and intralayer form adhesive solid bonding between the filaments and improve the mechanical properties [72]. Mechanical properties of intralayer and interlayer are different because of the different temperature gradients of both cases. And found that the time taken to deposition is less than the time from layer to layer. As a result, intralayer bond strength is more vital than inter-layer bond.

2.3 Prediction of mechanical property in FDM process

The FDM process's significant challenges in investigating the printing parameters over the effect on mechanical properties to improve in mechanical properties of porosity. Significantly neck size increases after reducing the porosity between the filaments. The necking phenomena are observed in Fig. 13.

2.3.1 Effect of porosity on mechanical properties

In the FDM process, observe the presence of porosity between the layer because this modulus of elasticity and strength of the parts decreases continuously, also, due to

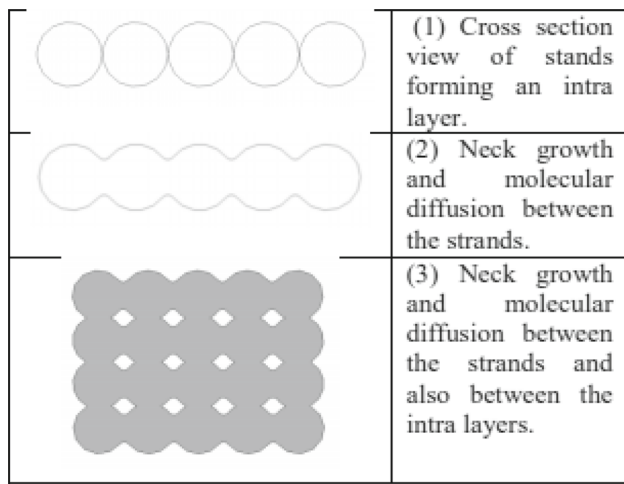


Fig. 11 Stage of bonding process in FDM [68]

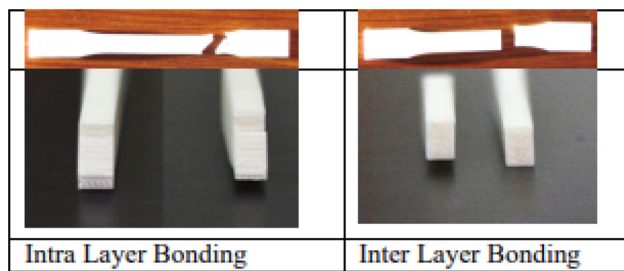


Fig. 12 variation in different mode of fracture because of intra and inter layer bonding under UTM [68]

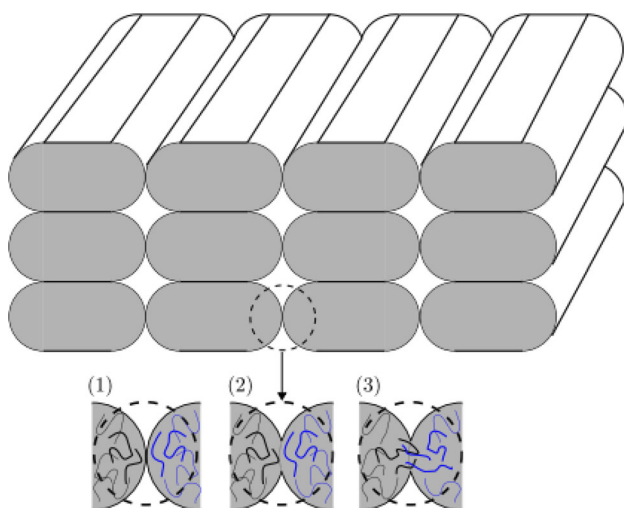


Fig. 13 Neck growth phenomena in FDM [22]

building orientation, when the void forms between the layers, reductions in neck growth dimension are relatively inferior to the mechanical parts strength elasticity. It is concluded that selecting proper building orientation and model of exposure plays a significant role in improving neck growth. Results in

bigger void size, less neck growth, and strength of the parts as shown in Fig. 14a, b and c.

The main parameter is the layer thickness that influences the reduction of the porosity between the filament, and strong molecular diffusion takes place at higher temperatures to improve the strength of parts quality [73] effect on printing process parameter on mechanical characteristics with porosity [74] in Fig. 14. The best parameter for obtaining specified mechanical attributes can be found from Fig. 15a and b. When the layer thickness is reduced from 0.3 to 0.1 mm, the void density decreases, and the mechanical characteristics improve. By increasing the printing speed then, void density slightly changes and has not much effect on mechanical properties. Printing speed significantly reduces the manufacturing time but affects the dimensional accuracy. Lower void density to obtain higher mechanical performance. It was increasing extrusion temperature to a slight change in the mechanical strength. Meanwhile, layer thickness went from 0.3 to 0.1, and void density decreased and enhanced mechanical properties' performance in the fused deposition modelling process [22]. Variable process parameters impact the bond strength in the FDM process. In this experiment using ABS material [75, 76]. The deposition of filament in the oblique direction, whichever is loading to the direction of the universal testing machine (UTM).

2.3.2 The variation in strength of bond with road gap

From the Fig. 16. Observed that the increasing road gap between the filaments started to decrease the bond strength. It is because of increase the road gap and decreasing the contact area between the roads.

2.3.3 Variation in bond strength with nozzle temperature

From Fig. 17. The influence of nozzle temperature on the strength of the bond. Meanwhile, nozzle temperature increases along with the bond strength. It started to fall after a specific value; at the beginning inter, road bond strength increases along with increasing the nozzle temperature because of the intermolecular solid adhesion bond uniting the road with not much change in shape and dimension. It may be degradation of the polymer after a certain period beyond a temperature, so the reduction in the bond strength is possible.

The Fig. 17 shows that when the bond strength increases with increasing the chamber temperature, the melting material is kept at a higher temperature for a more extended time [77]. The studies of the various parameter impact the quality bonding to improvement in the strength of final parts.

Investigation of the fundamental relationship between bond formation and mechanical properties of the final part. The parts' strength was evaluated by bonding between the

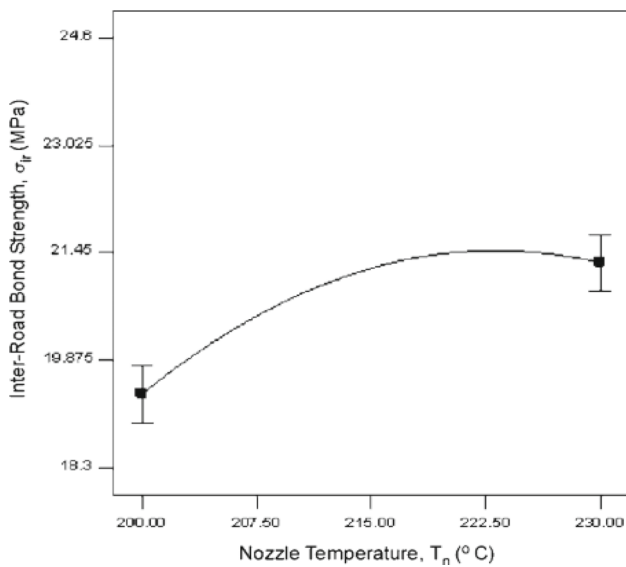


Fig. 17 Variation of bond strength with nozzle temperature [77]

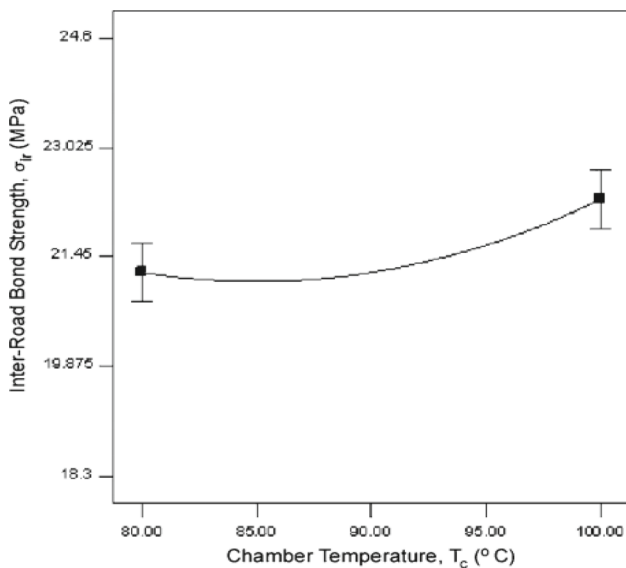


Fig. 18 Variation of inter bond strength with chamber temperature [77]

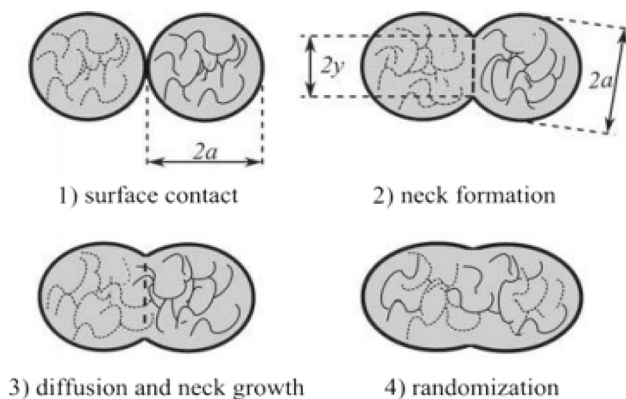


Fig. 19 Necking between adjacent roads [5]

mechanical properties on the bead contact between the adjacent polymers. The road bonding sintering process is used by using a viscous flow mechanism to improve the binding strength. Thermal energy drives the sintering process, and Sintering is significant. The function of the temperature of one road is at the interface over the other road to examine the bond strength.

AM controlled requires maintaining a constant road width and ensuring that the printed bead has sufficient thermal energy to create a strong bond with the material on which it is printed while varying feed rate with printing head velocity. When the bonding between the two adjacent roads resulting neck formation. The term "intra-layer" is defined that bond formation within a layer, and the other word is "interlayer," whereas bonding formation between the top and bottom layer. Neck growth describes the effect of bond creation over time. Suppose Increasing contact area, which means better bonding. Hence increasing contact area is significant to the highest strength for specimens with better dimensional stability. Dimensional neck size influences the strength and accuracy of parts [5]. Thermoplastic is very sensitive to temperature changes in the fused deposition modelling process. The temperature affects the part's strength in the additive manufacturing process. In this research, temperature influences neck growth formation. The neck is observed before the final pieces are manufactured. Neck size estimates the strength of the part [78]. Suppose two adjacent filaments form a bond resulting in neck formation. Two types of bond formation occur termed Intra and inter-layer bond formation. Whenever bond formation within a layer called interlayer and fond formation between the top and bottom layer is called interlayer bond formation. Phenomena of neck growth are affected by temperatures. Better bond strength observes when the contact area increases between the layers, resulting in a more considerable contact area and better bond strength.

The influence of dimensional neck growth enhances the dimensional part's strength and accuracy in the additive manufacturing process [79]—the expression of neck size in dimensionless quantity based on neck size to specified load. Dimensionless neck size is shown in the step-by-step process in the following Fig. 21a, b and c.

The variation of neck growth with temperature is shown in Fig. 22. When the temperature increases correspondingly, neck growth increases because interface temperature exceeds glass transition temperature, generally for ABS 110 °C. Because the molten material reaches the glass transition temperature and neck formation stops at this stage. Hence intermolecular diffusion occurs in the polymer to form a bond. When the temperature decreases results, no neck formation occurs. To obtain the desired parts strength with a prediction of neck size. The relationship between the neck growth and interface temperature to get effective bond formation.

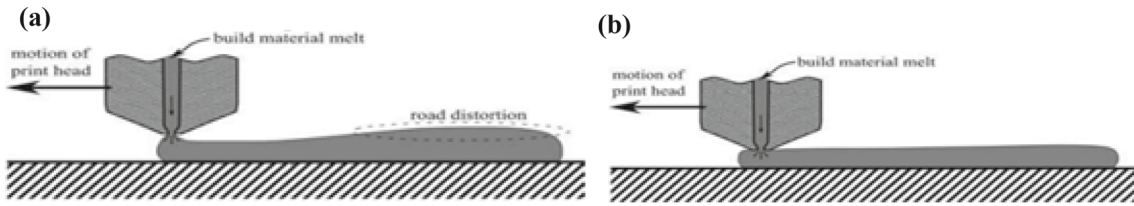


Fig. 20 (a) Print head and extruder road (b) print head without road [5]

Fig. 21 (a) Flow diagram for prediction of neck size, (b) Cross section of FDM parts loaded transversely, (c) Necking phenomena [80]

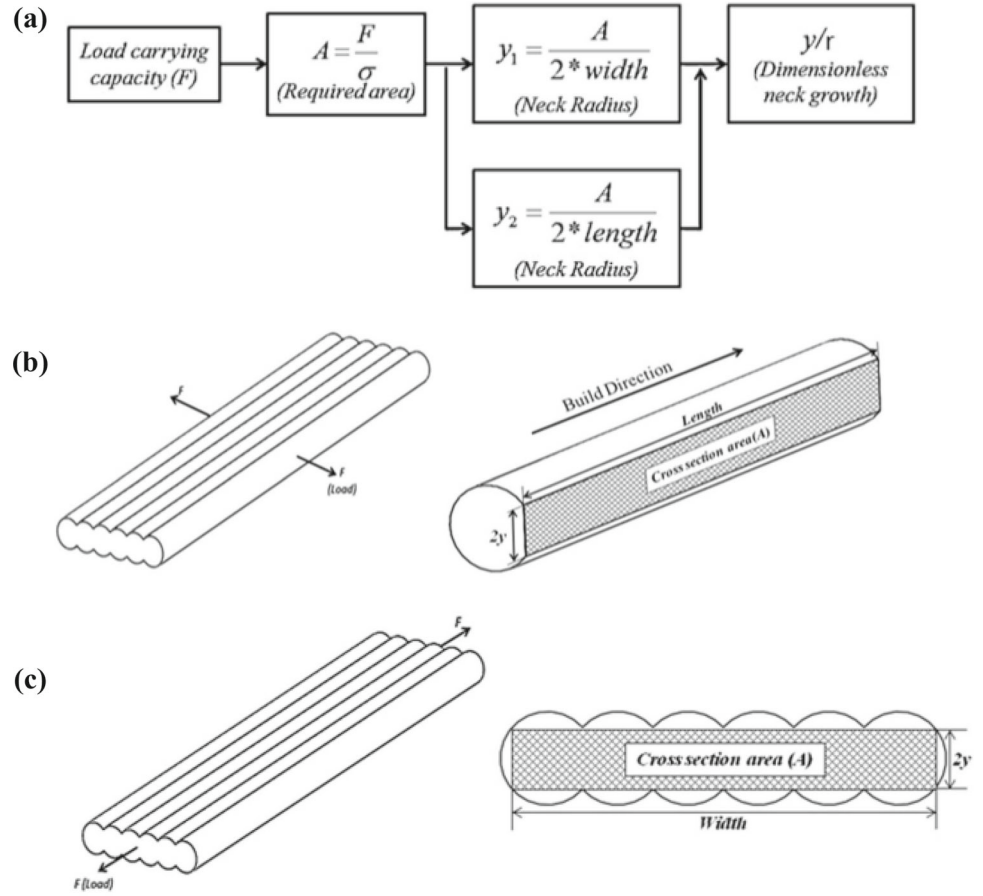


Fig. 22 Dimensional neck growth vs temperature [80]

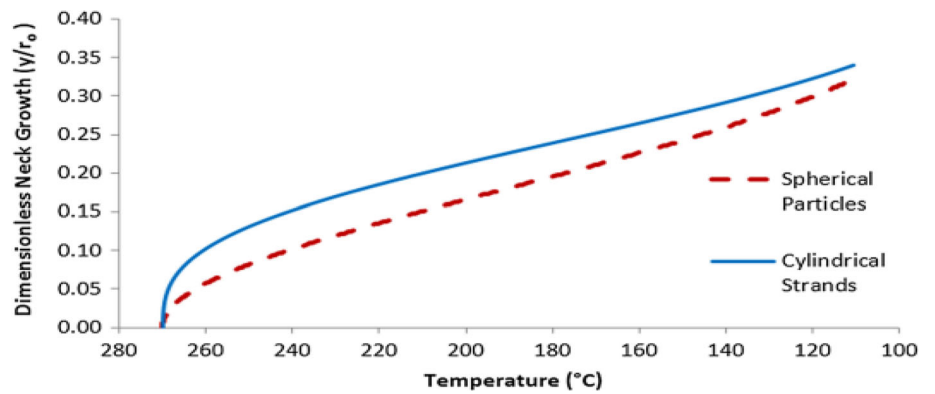


Fig. 23 (a) 245 °C Extrusion temperature, and (b) 260 °C extrusion temperature [80]

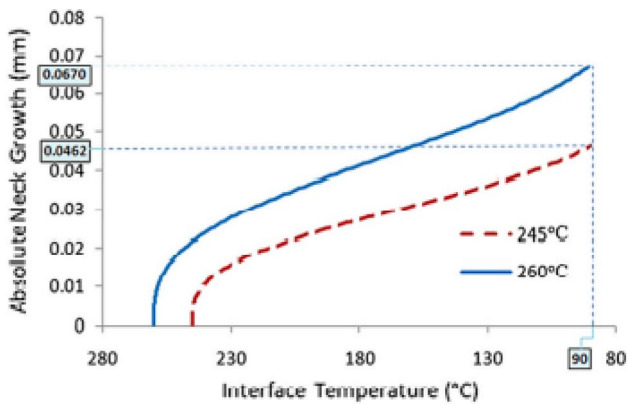
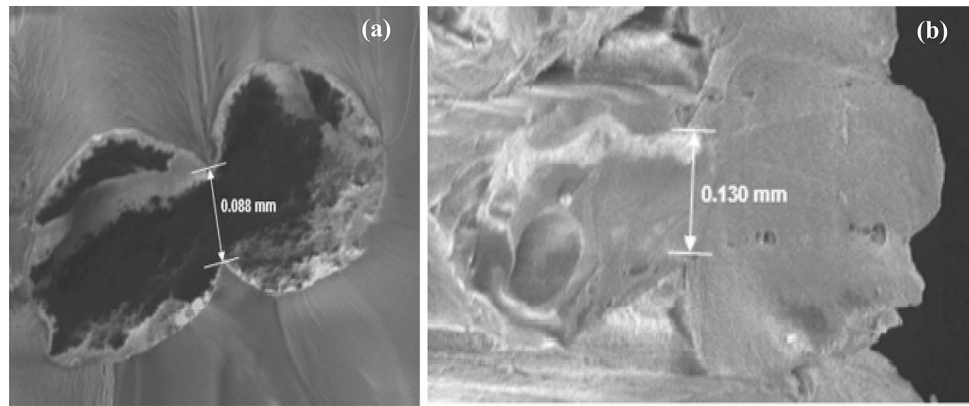


Fig. 24 Obtain graph from the extrusion temperature. at 245 and 260 °C [80]

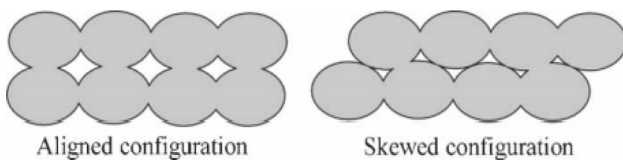


Fig. 25 Dimensional neck growth

The specimen of manufacturing parts is obtained with two different extrusion temperatures, such as 245 and 260 °C. Both samples were tensile tested in UTM. During the testing specimen fracture and observed SEM for the bond formation as shown in Fig. 23a and b.

2.3.4 Variation in absolute neck growth with interface temperature

It was found that from Fig. 24. When the extrusion temperature rises increases, the neck size. Intermolecular solid diffusion occurs between the two adjacent roads—desired neck size obtained with extrusion temperature. When increasing the extrusion temperature correspondingly interface temperature rises, improving dimensional neck size [80].

2.3.5 Effect of neck formation on parts surface finish

The fabricated parts of surface roughness are measured using a device called Talysurf. The tip of the Talysurf stylus movement all over the top surface of the cross-section to obtain deviation on the surface profile or to measure the surface roughness in the measurement direction. Surface roughness (R_a) originating at machine output results in an arithmetic average to exit the roughness profile from the centreline within the estimated length.

$$R_a = \frac{1}{l} \int_0^l y(x) dx \tag{23}$$

where R_a surface roughness of the profile average, $y(x)$ is the height of the surface profile and l is length of sample [81].

In the literature survey, the surface finish in the fused deposition modelling Process is influenced by various parameters. One of the most substantial concerns in the FDM process nowadays is boosting quality surface finish. The neck growth configuration is shown in Fig. 25. The critical parameter for increasing surface finish, likely road gap, nozzle temperature, and liquefier temperature as shown in Fig. 26. The main parameter is road gap increases with an increase in the surface roughness of objects. However, reduced road gap decreases peak to valley height and improves surface roughness, as shown in Fig. 26.

2.3.6 Variation in surface roughness with nozzle temperature

When nozzle temperature is kept higher significantly better surface finish is observed in the fused deposition modelling process. Surface roughness slightly varies with liquefier chamber temperature, and road gap and nozzle temperature play a significant role in improving surface roughness over the chamber temperature, as shown in Fig. 27. When increases nozzle temperatures and decreasing road gap result in a decrease in surface roughness. Lower road gap along with

Fig. 26 Surface roughness vs. road gap [77]

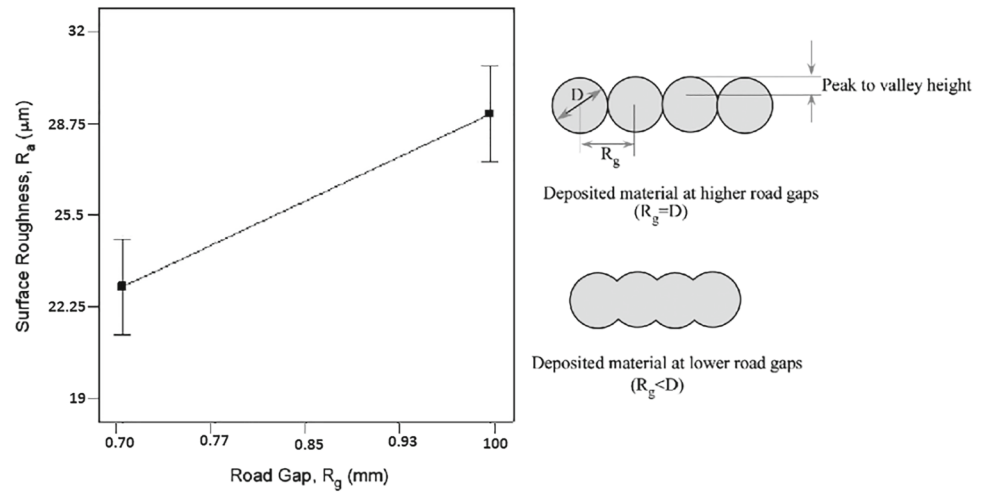


Fig. 27 Surface roughness vs. Nozzle Temperature [77]

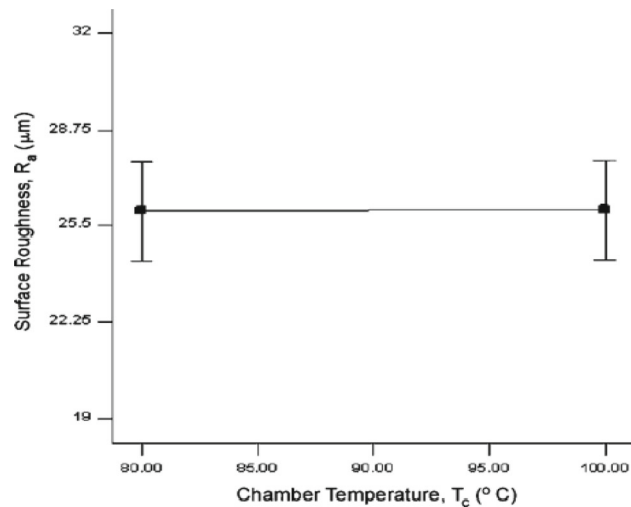
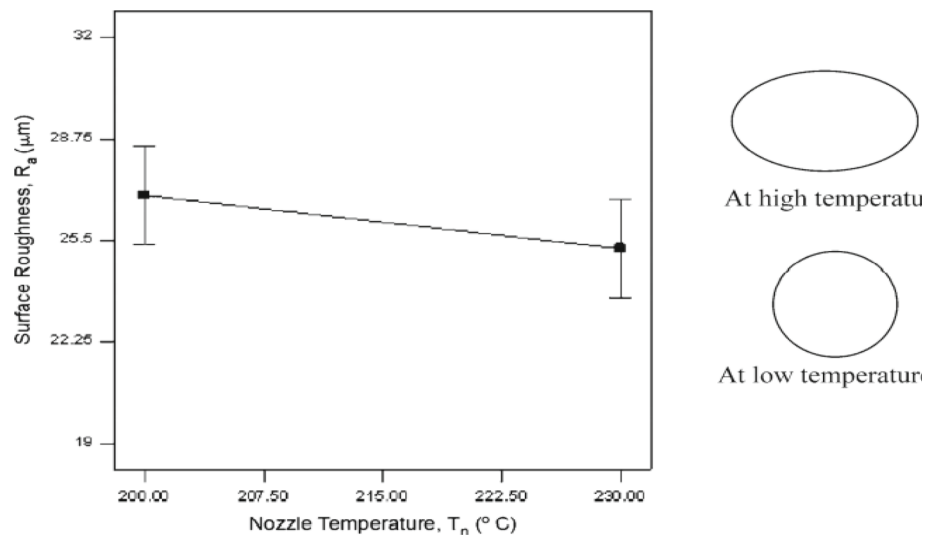


Fig. 28 Surface roughness vs. chamber temperature [77]

the higher temperature of nozzle is desired to get a better surface finish in addition to the strength of parts with accuracy.

2.3.7 The effect of chamber temperature on surface roughness

When increasing the chamber temperature results in surface roughness is not much change. It indicates that chamber temperature is less effective over surface roughness comparatively nozzle temperature, as shown in Fig. 28.

2.3.8 The influence on nozzle temperature and road gap on surface roughness

It is seen in Fig. 29. When nozzle temperature increases and road gap decreases, that results in the decline of the surface roughness. A low road gap and high nozzle temperature are desirable for better surface finish and strong bond formation [77].

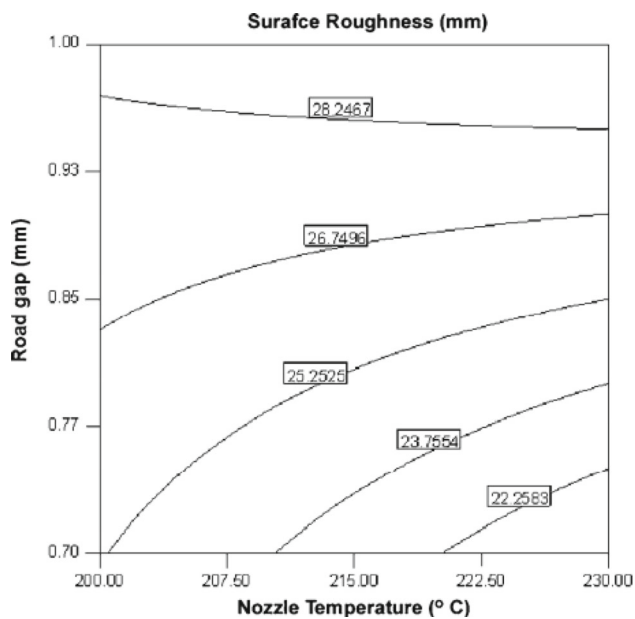


Fig. 29 Surface Roughness vs. road gap and nozzle temperature [77]

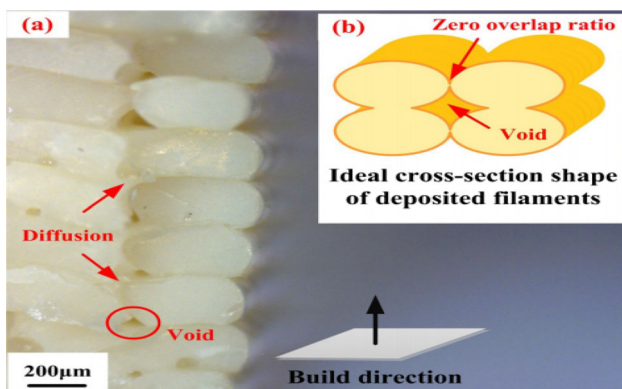


Fig. 30 (a) Zero overlap ratio, and (b) Cross-sectional shape of ellipse [26]

The heat-resistant resin is used in FDM for experiments. It is poly ether-ether ketone (PEEK), which possesses a high melting temperature of 343 °C. This thermoplastic polymer has an excellent advantage to improvement in the surface roughness. It was seen that the most substantial tensile strength of parts with 100% infill density. Because of high melting, platform temperature is higher. So, components prevent deformation and warping [82].

The cross-sectional profile is observed to be an ellipse, as shown in Fig. 30a Zero overlap ratio and the Fig. 30b The shape of the 3D printed PEEK display the different porosity with ellipse even with the same printing settings, extrusion material flow, and overlap gap. An analysis from Fig. 30a and b.

It is clear that a bit of bond is produced between the layer surface and touching the surface to diffuse because of surface

tension operated by the material's thermal properties. Due to this void between the adjacent filaments appeared. It is not significant for the Neck growth in the FDM process; it occurs due to insufficient energy to accelerate the polymer to move. And therefore, heat resistant mechanisms need high heating temperature further to improve dimensional neck size formation. Neck size is desirable to estimate the bonding quality. The heat-resistant resin in the FDM process is significant for improvement in surface finish and declining overlap between the surface roughnesses. For the experiment, we fixed the zero-overlap interval. The bond formation between the filaments by molecular diffusion arrangement is shown in Fig. 31a, b, c and d The shape of the filament is an ellipse.

In the FDM process, PEEK is used to perform several experiments to improve accuracy and surface roughness [83]. Comparing the result experimentally as well as calculated results. Investigation of several parameters during printing, likely temperature of nozzle, platform temperature, layer thickness, and printing speed for better surface finish and morphology [11].

Variation in surface morphology of PEEK printed parts, experimental and model results of surface roughness with the nozzle temperature 340 to 420 °C.

From Fig. 32a, b and c observe that when increasing the nozzle temperature, the results in void size appeared to be small. In this investigation, based on the thermal physical properties, when the rising temperature enhances the kinetic energy of the molecular moment, strong diffusion takes place between the molecules due to this void disappearing from the filament surface.

When nozzle temperature increases 380–420 °C results decrease void and surface roughness drops. We observed that nozzle temperature's impact is more than the build platform temperature on the surface roughness. The main reason behind the temperature of the nozzle is a function of thermal energy to supply heat. Thermal energy calculates the kinetic energy of molecule movement. Hence building platform temperature impacts the higher than the ideal kinetic energy from the first molecular motion diffusion time to a larger region. Also, similar phenomena were found in platform temperatures varying from 220 to 300 °C, while rising the platform temperature decreases the roughness and void formation, as shown in Fig. 33a, b and c.

Surface morphology of PEEK printed parts varies with printing speed, experimental and model results of surface roughness varying with printing speed ranges from 5 to 25 mm/s as shown in the Fig. 34a, b and c.

Increasing the printing speed from 5 to 15 mm/s results in dropping the surface roughness. Then further increasing the printing speed continuously increases the surface roughness because the heat transfer results in the surface roughness between the depositions of filament over the build platform [84].

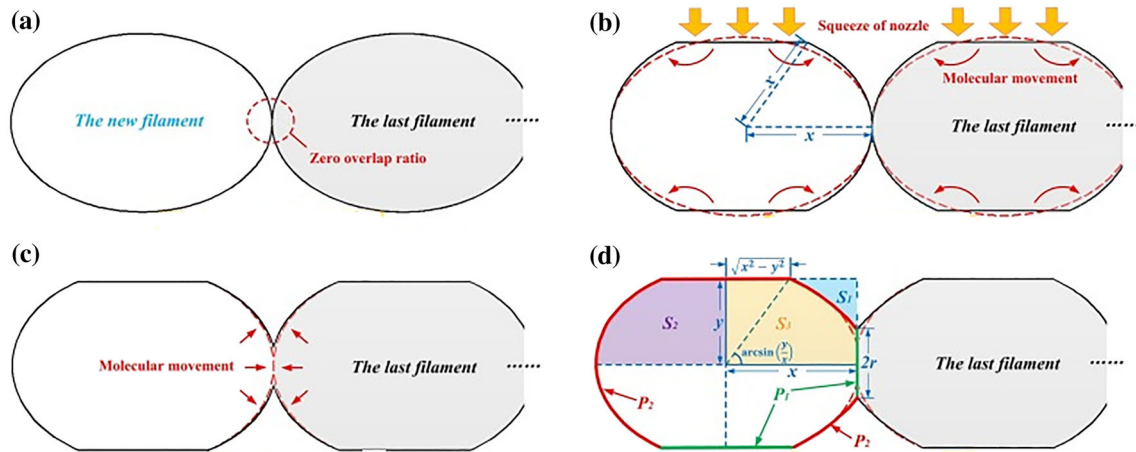
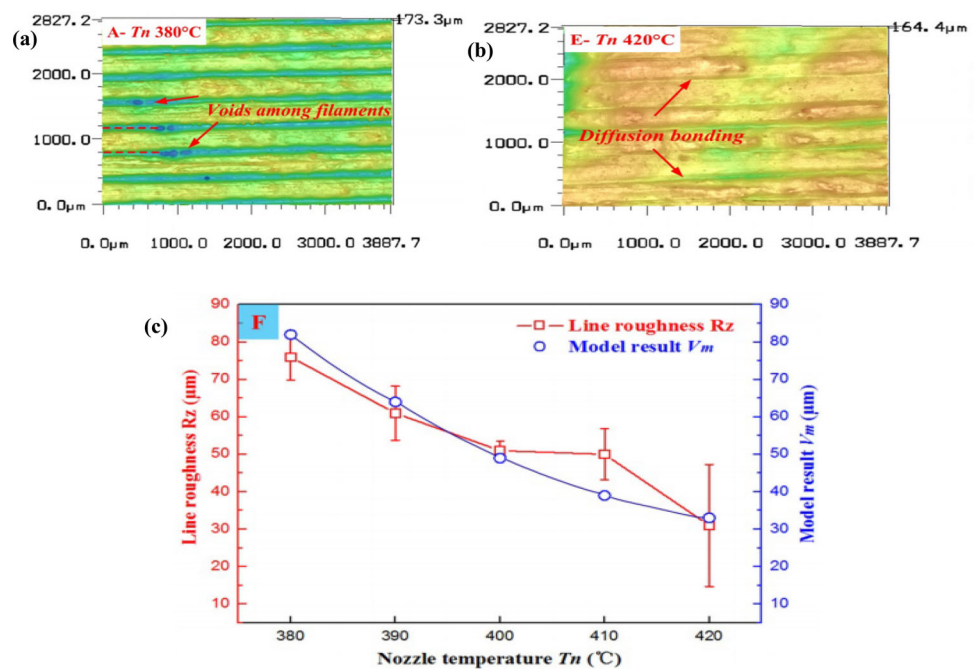


Fig. 31 (a) Ideal cross-sectional shape, (b) Flating effect of nozzle, (c) Contacting and wetting, and (d) Diffusion and neck growth [26]

Fig. 32 (a) Morphology at T_n 3800 °C, (b) Morphology at T_n 4200 °C, and (c) Line Roughness vs Nozzle Temperature [26]



In the surface morphology investigation of printing parameters, the term stacking indicates that a large quantity of filament deposited on the printing surface occurs due to the nozzle deposited more an extended period at a lower printing speed. Surface roughness is higher enough at a higher printing speed, and the nozzle squeezing effect on surface roughness was observed and considered [85].

Surface morphology of PEEK printed parts varies with layer thickness, experimental and model results of surface roughness change with layer thickness ranges from 5 to 25 mm/s as shown in the Fig. 35.

It is different to affecting the surface roughness by temperature. When increasing the layer thickness results in increasing the surface roughness.

It shows that the void size is more prominent, whereas increasing the thickness of the layer affects the roughness. It means that increasing the layer thickness increases void and surface roughness. And nozzle squeezing at lower Layer thickness due to high viscosity and poor fluidity that worsen the surface roughness. The recommended layer thickness of 0.15 mm is the best surface finish [26]. The literature survey reveals that the final FDM parts have poor surface properties; likely, surface roughness, dimensional correctness, and even minor mechanical properties are all factors to consider. Generally, FDM parts require post-processing to enhance the quality of surface finish [9]. It is introducing new techniques to improve the surface properties. The chemical treatment technique is used because it has a low initial cost investment and advantages the surface roughness effectively. Based on

Fig. 33 (a) Morphology at T_p 2200C (b) Morphology at T_p 3000C and (c) Line Roughness vs Platform Temperature [26]

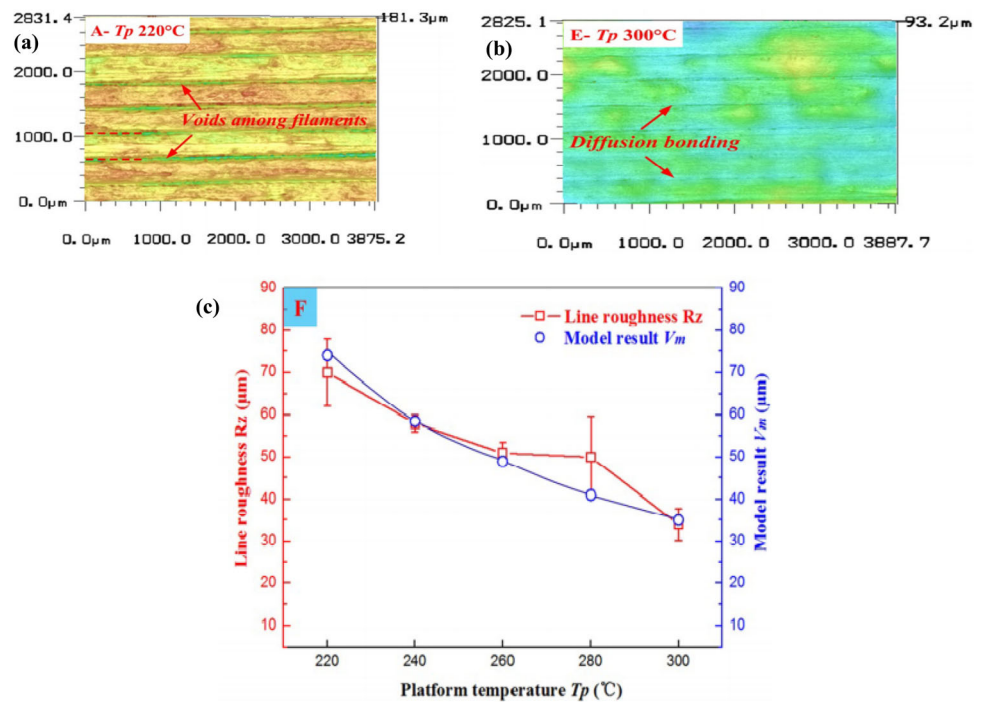
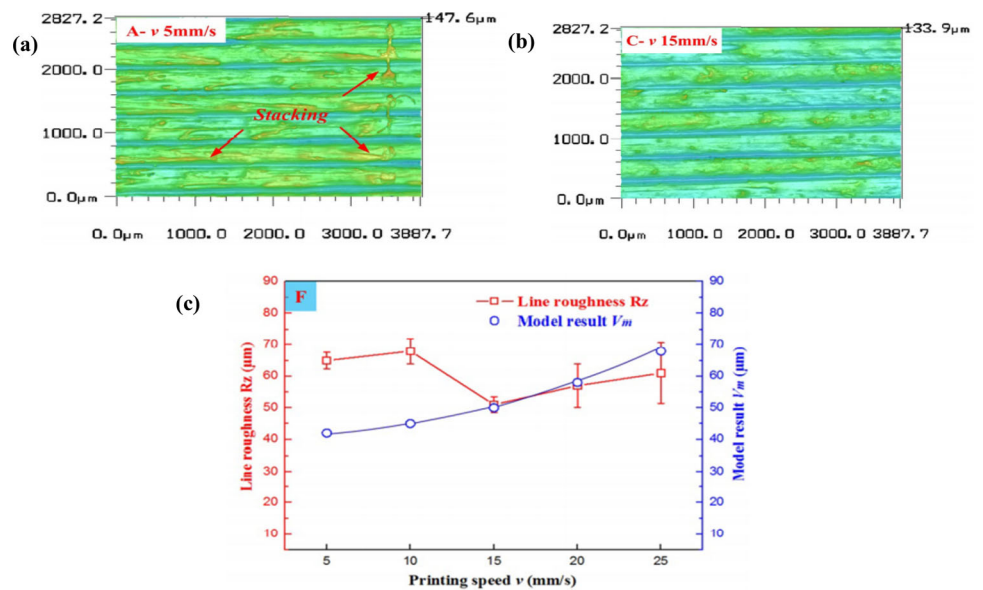


Fig. 34 (a) printing speed at 5 mm/s, (b) printing speed at 15 mm/s, and (c) Line surface vs printing speed [26]



the performance of chemical treatment technique to effect on surface roughness, impose it. Surface roughness can be improved using a combination of Chemical approaches and 3D characteristics such as layer thickness, infill density, and orientation. The chemical treatment process uses Nano clay to smooth the surface roughness. Nanoparticles deposited via chemical and solvent form on printed FDM parts to enhance the surface.

The filament material is used as ABS to produce parts, and post-processing is used in both Nano clay and dimethyl ketone (DMK). It is very cheap and widely used in the

chemical treatment process. The Nano clay and DMK are appropriately mixed and immersed in the parts to obtain a smoother surface. The nanoparticle can improve the mechanical properties [86, 87]. The primary objectives of this study were to analyze the effect of post-processing on FDM parts to attain the desired surface qualities. For practical use in industrial applications such as assembly parts, rapid tooling, and castings. An investigation of the chemical treatment process of surface roughness found that more surface finish at the lower thickness Shown than higher layer thickness [10, 88] as shown in Fig. 36.

Fig. 35 (a) Layer thickness at d 0.1 mm, (b) Layer thickness at d 0.3 mm, and (c) Line roughness vs Layer thickness [26]

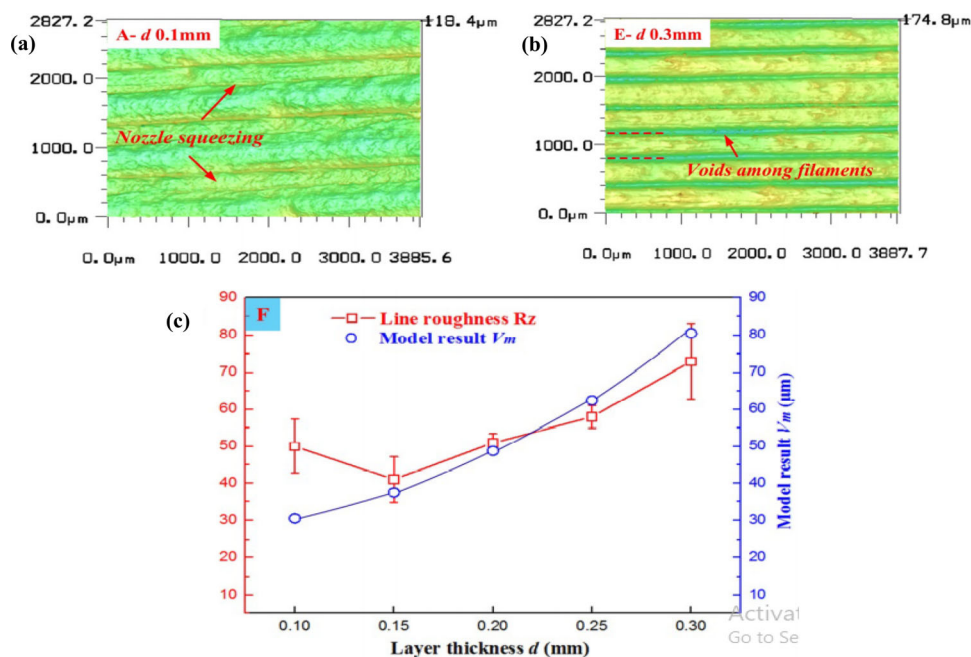
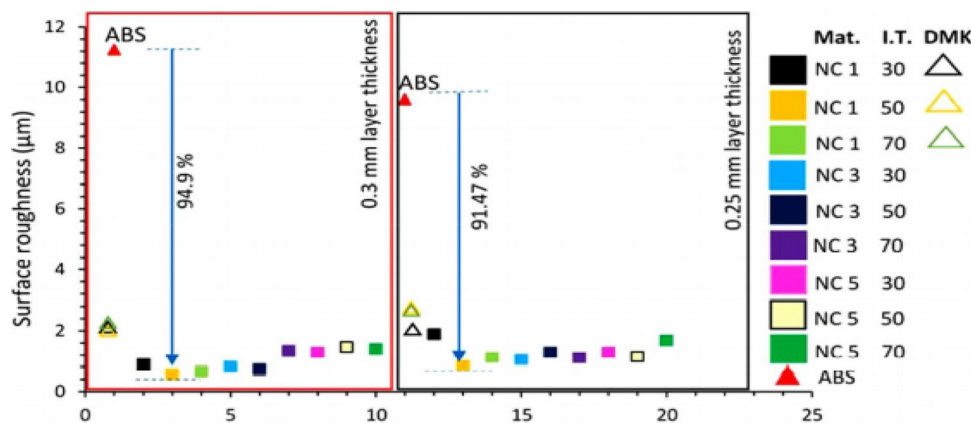


Fig. 36 Roughness of the surface before and after the surface modification method (Mat. Material; I.T. Immersion time) [89]



It reported that at lower layer thicknesses, the consequence of lower stair and height of peak to valley of a raster is smaller than at higher layer thicknesses. When using the chemical treatment techniques of NC and DMK on FDM parts specimen, the substantial reduction in surface roughness and achieve the desired better surface properties at a lower layer thickness of 0.25 mm to obtain 91.7% and a higher layer thickness of 0.30 mm to acquire 94.9% respectively.

Achieve the desired surface due to the interaction of ABS with DMK solvent solution. Due to the staircase effect on FDM parts. When the DMK with the outer surface of FDM parts, soften the outer layer parts. The sliding of the polymer chain, one over another, breaks the bond, and the void gets filled. When the solvent evaporates, the polymer gets solidified to this phenomenon substantial reduction in surface roughness, as shown in Fig. 37.

The immerse time and Nano clay content did not significantly increase the surface roughness over the declining modified surface roughness. To achieve the significant surface roughness at a low quantity of clay with moderate immerse time over both thicknesses of layer [89, 90] as shown in Fig. 38. When Results of layer thickness on the microstructure 1.58 and 0.72 mm cross-section of specimen. It was found that there is no significant effect on grain size or microstructures between both samples, and chemical treatment techniques din not substantial. The average surface roughness of both specimens is similarly observed at a grain size of 40 μm , as shown in Fig. 39.

The result of surface roughness in mechanical characteristics in FDM parts, when the thickness of components is decreased, relatively the area of the specimen grows as the effect of surface roughness on mechanical properties grows. It was recognized that reduction in the layer thickness of the

Fig. 37 Surface smoothing mechanism for 3D printed items [89]

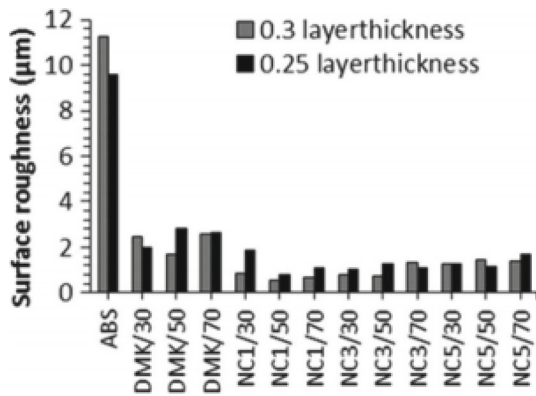
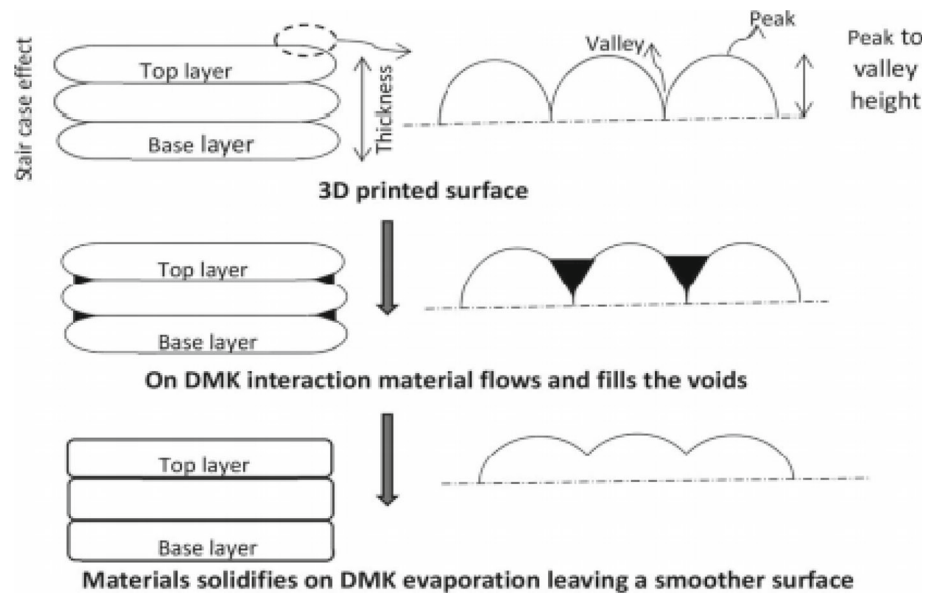


Fig. 38 Effect of layer thickness on surface roughness [91]

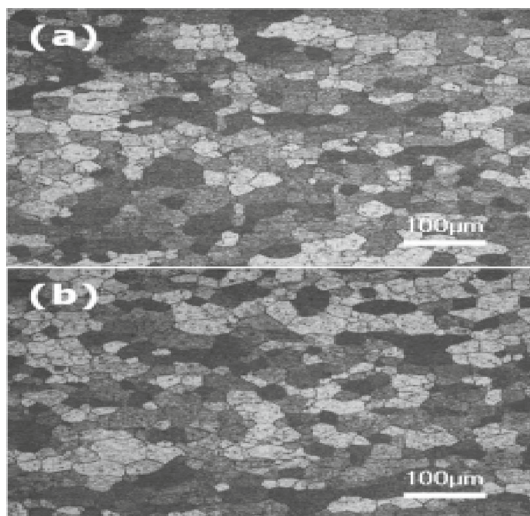


Fig. 39 Microstructures of (a) 1.58 mm Al sheet surface and (b) chemically etched 0.72 mm Al sheet surface [91]

parts' surface roughness enhances because of that tensile and yield strength fall when the number of grain size comparatively decreased. The size layer thickness of both graphs is 1.58 and 1.04 mm, respectively [92], as shown in Fig. 40.

And also, ductility decreases. For smaller thickness, neck size is observed less due to plastic deformation not diffusing. Dent localized necking is a method to enhance neck size in the direction of thickness in thick specimens. It is observed later the uniform elongation. Hence plastic deformation widely occurs, and neck formation increases. In the fragile sample, no necking appeared, uniform elongation decreased, and surface defects, including surface roughness, initiated crack. In mechanical properties, the effect of size and surface roughness must be considered when material and parts are reduced [91]. The familiar surface defects in the fused deposition modelling process are staircase, burrs, chordal effect, and any misprint of the beginning and end of filament deposition.

The survey of this paper found that the temperature of liquefier higher than the material of the filament is more in molten or fluid states desired for surface finish. Layer thickness increases with surface finish. The build orientation is 70 deg. And layer thickness of 0.007 inches is desirable for surface finish. Surface finish is not significant in terms of a better quality of parts but is also considered to reduce post-processing time and cost. When the fused deposition modelling (FDM) process produced pieces, it was found that the always space amid the neighbouring filaments, as shown in Fig. 41a and b.

From the Fig. 42. When increasing the increasing layer thickness with the effect of stair case increasing due to void increasing between the adjacent roads and results in increasing the surface roughness [94].

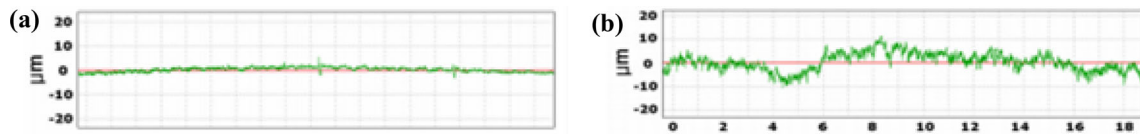


Fig. 40 (a) Surface roughness at thickness 1.58 mm, and (b) Surface roughness at thickness 1.04 mm [91]

Fig. 41 (a) Road Width and Layer thickness, and (b) Layer showing roads and the air gap between roads [93]

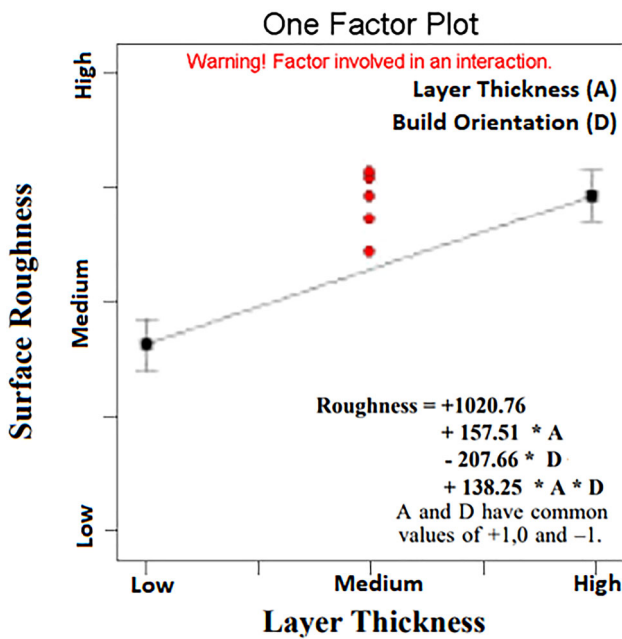
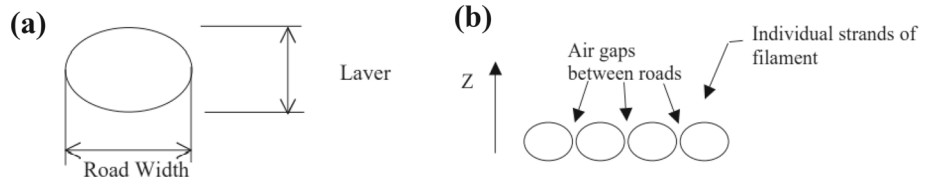


Fig. 42 Surface Roughness Vs. Layer Thickness [93]

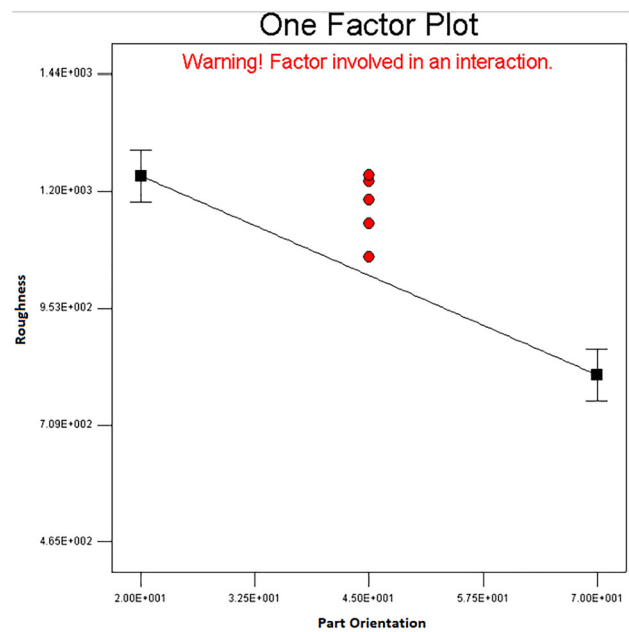


Fig. 43 Surface Roughness vs. Part Orientation [93]

From the above Fig. 43. When the parts orientation at lower angles which affect the top layer each other by stacking and results in increase the surface roughness [95, 96].

When the offsets occur between roads which affects the surface roughness on a shallow inclination with Steep as show in the Fig. 44. In this found that the better surface finish at lower layer with a high part orientation [93]. The neck formation produced when two adjacent filament formed bond and bridge formation that phenomena is called necking as shown in the below Fig. 45a and b.

From Fig. 46. It was discovered that the surface roughness increases when the layer thickness grows, rising due to the dimensional size of the void and the air gap being more significant. When the layer thickness decreases, void size disappears between the filament and gets smoother surface roughness [97]. An investigation found that factors affect surface roughness and parts accuracy by the layer thickness

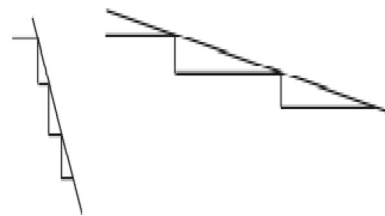


Fig. 44 Offset layer [93]

dimension. The desirable parameter for the surface roughness is low deposition speed, low infill density, and lower layer of thickness [98, 99], as shown in Fig. 47.

Layer thickness is significant to investigate for suitable surface finish and parts accuracy. Optimize the 3D printing process parameters. It obtains a considerable dimension of parts accuracy and good surface roughness. Results from

Fig. 45 (a) Neck Formation, and (b) Neck growth evolution at constant Temp.220 °C with interval of time of ABS [97]

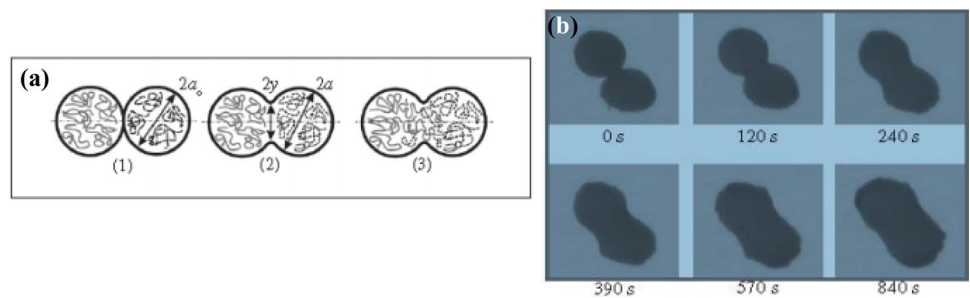


Fig. 46 Effect of layer thickness on surface roughness [97]

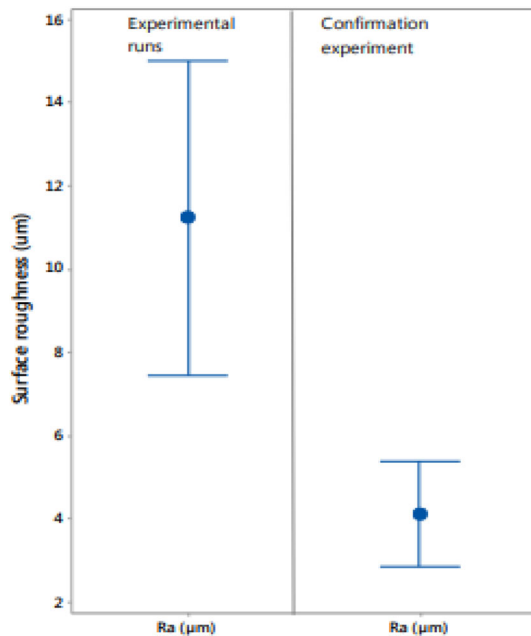
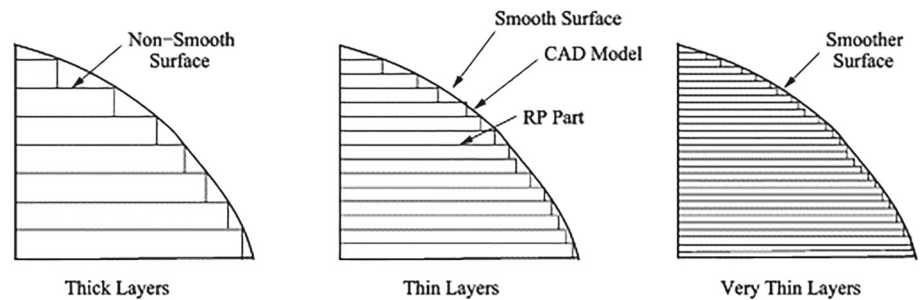


Fig. 47 Surface roughness [81]

Fig. 45 Indicate that the lesser thickness is best for accuracy and roughness [81, 100].

Surface roughness as a function of layer thickness, road width, raster angle, and air gap as shown in Fig. 48 below.

From Fig. 48. We have seen that the medium layer thickness is better for surface roughness. If increases the layer thickness increases, the surface roughness. A layer thickness of 0.2–0.3 mm is optimum for surface roughness. When initially increasing the road width, that decreases the surface roughness at medium roads width that is increasing the

surface roughness [101]. Changing the raster angle slightly drops the surface roughness [102]. And the negative air gap affects the surface roughness, and when increasing the air gap is positive in the fused deposition modelling process, better surface roughness and part strength are desired [27].

2.3.9 Effect of neck formation on part accuracy

One of the biggest concerns in the fused deposition modelling process is accuracy. Accuracy is primarily affected by the manufacturing parameters, and the orientation directly influences the accuracy and repeatability of FDM parts. The accuracy of other plastic technology is higher than building FDM parts [97] and, at the same time, enhances the precision of dimensioned elements and improves the mechanical qualities of the parts. The mechanical characteristics of the FDM process are not particularly connected to part accuracy. And more significant size object is more accurately manufactured in FDM. The dimensional accuracy is determined by the average deviation from all inspected dimensions. The relationship used for the dimensional accuracy is expressed from Eq. (24).

$$Kd = \frac{Klen. + Kw1 + Kw2 + Kh}{4} \tag{24}$$

KD is the coefficient of dimensional accuracy, and Klen is the length. Kw1, Kw2, width at 1 and 2. Oh, thickness. It was observed that lower accuracy results in a higher value of dimensional accuracy coefficient. So desired accuracy is achieved at the lower coefficient of dimensional accuracy. The coefficient of repeatability is determined by the average

Fig. 48 (a) Surface finish vs. layer thickness, (b) Surface finish vs. Road width, (c) Surface finish vs. Raster angle, and (d) surface finish vs. Air gap [27]

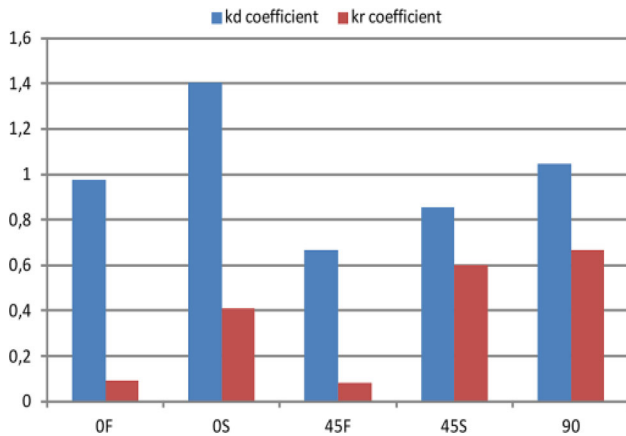
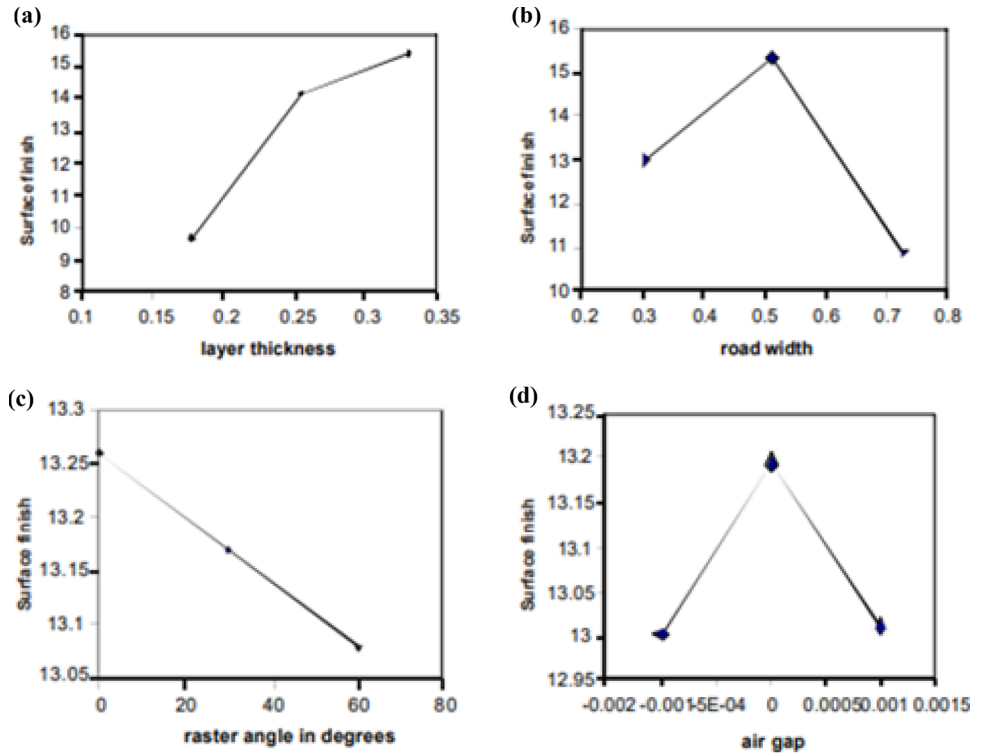


Fig. 49 Accuracy and repeatability coefficients for FDM samples [103]

difference between the accuracy coefficients. The repeatability formula is expressed in (25).

$$Kr = \frac{(K1 - K2) + (K2 - K3) + (K3 - K4)}{3} \quad (25)$$

where Kr is the repeatability coefficient and K1, K2, K3 are the accuracy coefficient. In the expression observed that the higher the coefficient results in lower the accuracy.

From the Fig. 49. Observe that the lower the value of accuracy and repeatability coefficient results in higher the value of accuracy. Achieve the desirable value at a lower coefficient and better accuracy. When the accuracy of FDM

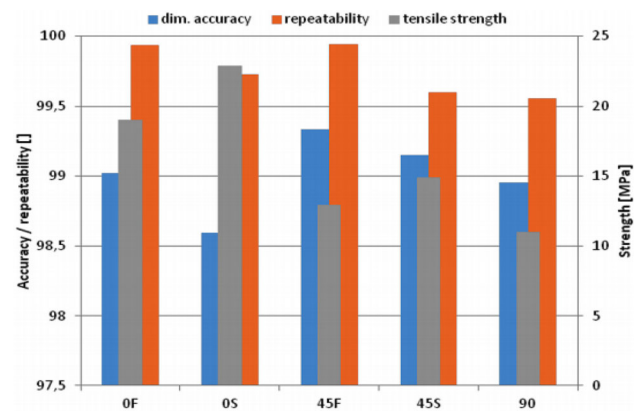


Fig. 50 Strength and Accuracy with FDM parts sample [103]

parts increases results in an improvement in parts strength observe in Fig. 49. From Fig. 50 because the increasing accuracy means bonding quality between the adjacent filaments is better. The higher the accuracy value, the tensile strength achieves [103].

In the FDM process, build-orientation, infill density percentage and infill patterns, extrusion temperature and layer thickness, and printing speed are all influenced by part perfection in the FDM process. The orientation of the building has a significance on Dimensional accuracy.

Layer thickness and extrusion temperature are more critical than infill % and pattern, printing speed, and dimensional accuracy of FDM objects in enhancing dimensional accuracy.

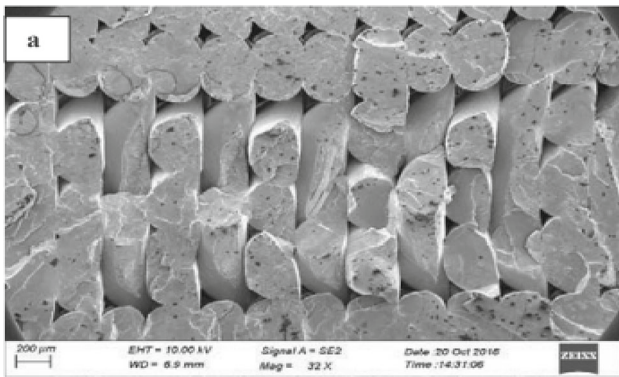


Fig. 51 FDM parts with void formation [104]

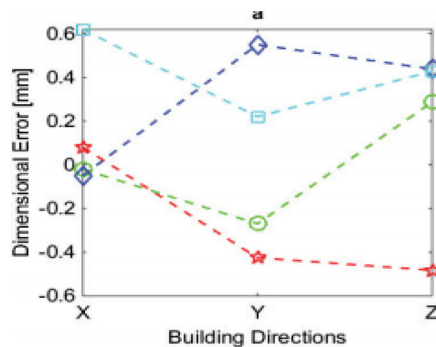


Fig. 52 Accuracy vs. Building direction [104]

It has to keep the aligned orientation rather than building direction and lower the extrusion temperature and layer height. An investigation of dimensional accuracy in FDM parts [13] is shown in the Fig. 51. That porosity and void are still present in the FDM parts even if the infill density is 100%.

From Fig. 52. It is clear that building direction influence the dimension of parts accuracy. Due to variation in positioning of fused deposition modelling (FDM) extruder from the Fig. 53. It was seen that there is not significant to affect the infill percentage and pattern on the dimensional accuracy pattern [105].

Dimensional accuracy was dependent on the extrusion temperature. When the extrusion temperature increases results in an increase the dimensional accuracy because when rising the extrusion temperature, the molten filament is more in a liquid state or (fluid state) as shown in Fig. 54]. This analysis found one of the significant roles of layer thickness. Along with surface roughness, layer thickness impact's part dimension accuracy. Low deposition speed is a desirable feature for dimensional accuracy. The average percentage of infill density and a higher layer of consistency and surface roughness are low deposition speed, low infill density, and lower layer thickness. Layer thickness is significant to investigating suitable parts' accuracy [106], as shown in Fig. 55.

we controlled the optimum parameters experimental for analysis of dimensional accuracy. Such as ΔL , ΔW , Δt and T represent Changes in length, width, and thickness to indicate the need for experimentation. Because the essential parameter sets for dimensional accuracy and surface finish differ, determining the combined optimum parameter set is challenging, and the desirable properties exist [81].

The fused deposition modelling process produces parts and tests the specimen in the paper survey making the specimen in two groups. The first is a cylindrical specimen, and a bone tensile specimen is made. Hence, the cylindrical specimen parts were produced with three colors and different building orientations. Meanwhile, the raster angle and layer thickness were set to 45/135, and 200, respectively, in mm. And dog bone tensile specimen is produced by the three-layer thickness and three building orientations, and three raster angles shown in Fig. 56a and b. The infill density was used 100% while producing the parts, and the thermoplastic material is PLA.

From the figure of the cylindrical specimen, due to a tilt of 45 deg. Angle so that support material used for the cylindrical model. The dimension of the sample has a diameter of 8 mm and a height of 15.2 mm; meanwhile dog bone specimen has geometry obtained according to ISO 150 mm long, 20 mm wide, and 4 mm thick. The cylindrical model's dimensional accuracy is shown in the figure below. This test compares the value length and diameter with different printing orientations and colors. It is found in the figure that the specimen produced an angle of 45 deg. When Reduction in dimensional accuracy with increasing the standard deviation error bar. It occurs due to the tilted position of layer orientation at an angle of 45 deg. Also, another horizontal and vertical cylindrical specimen was observed with high dimensional accuracy [108].

From Fig. 57a and b. The dog bone prototype testing compares the accuracy over the thickness and width dimension of different printing parameters, likely layer thickness, printing orientation, and raster direction. Except for the layer thickness of 100-micron meter, other has high dimensional accuracy observed in the graph.

In the case of width, there is significant accuracy on flat orientation and upright orientation except for the on-edge exposure. There is a slight reduction in accuracy in the on-edge direction due to increases in layers' thickness. In the case of thickness, 300-micron meter observed the lower accuracy than width because layer thickness increases with decreasing the accuracy reason to the formation of the void. Results show that the higher the layer thickness, the greater the accuracy [107].

In material extrusion, the entire process mainly depends on combining thermal–mechanical methods. Controlled of effective properties and mesostructured by printing parameter process [109]. The material extrusion process is primarily concerned with some influential process factors such as

Fig. 53 (a) Dimensional error vs. infill percentage, (b) Dimensional error vs. infill pattern [104]

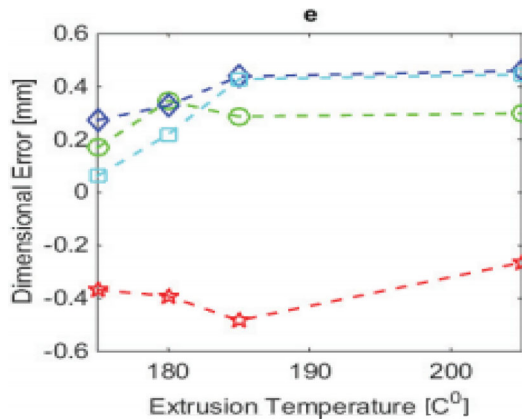
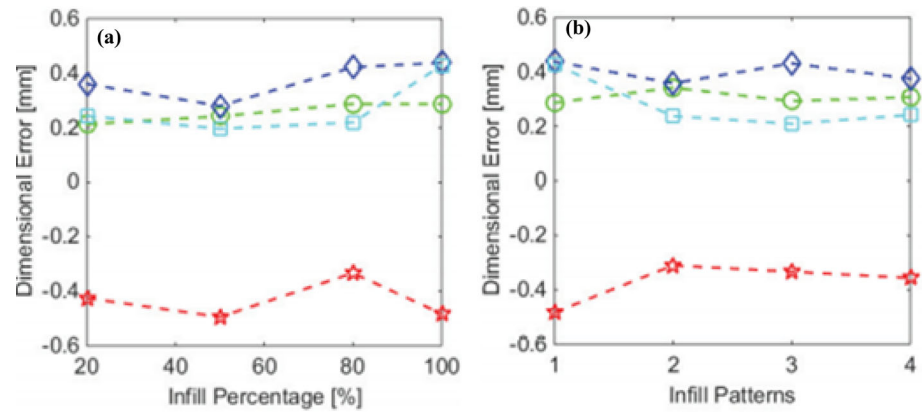


Fig. 54 Dimensional error vs. Extrusion Temperature [104]

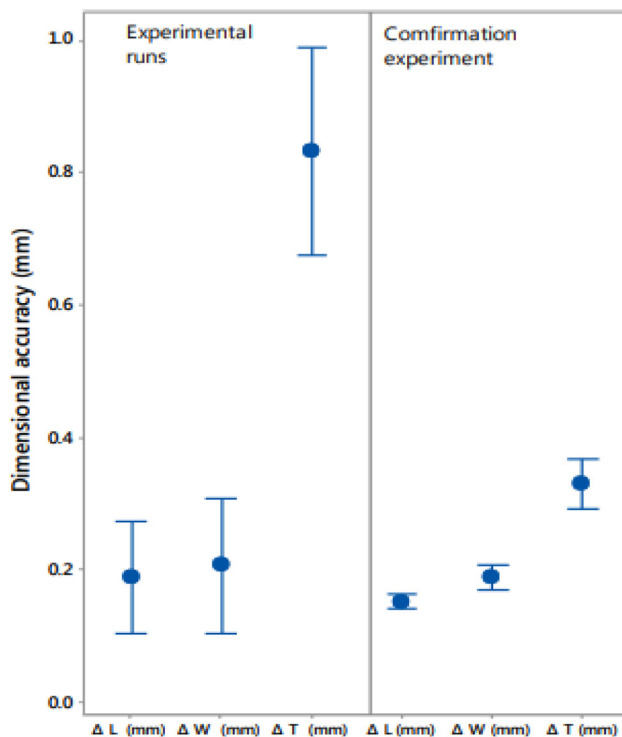


Fig. 55 Dimensional accuracy with dimension [81]

extrusion temperature, printing speed, layer thickness, and flow rate [15].

Investigation of process parameter effect on structure and performance unidirectional and aligned in the material extrusion process. Two-step Prediction process on mesostructured printing parameter and final mechanical properties [110]. The material extrusion sequences are expressed in Fig. 58a–f. From Fig. 59. It is found that the comparison of strand dimension and product is fairly good because porosity is lesser. It was seen from the survey strand temperature decreasing as left the nozzle tip and resulted in lower filament deposition temperature compared to extrusion temperature.

This porosity enhances and decreases the dimensional accuracy [6]. When producing parts, the infuse deposition modelling (FDM) process requires more parameters and optimization to obtain the desired dimensional quality of components [111]. Layer thickness, air gap, raster angle and bead, and road width are some of the process parameters shown in Fig. 60—raster angle between the two successive layers.

The air gap is the distance along with adjacent roads of the fused deposition modelling process. When the air gap is 0 (zero) meant to be slightly in contact between the two streets. Meanwhile, the air gap was positive, resulting from no connection between the roads to get loose structures packed quickly. The negative air gap requires a more extended period to build the dense network because it partially occupies the two routes over the same space, as shown in Fig. 61.

The effects of road width, raster angle, layer thickness, and air gap on dimensional accuracy as shown in the Fig. 62a–d.

From Fig. 62a–d. The medium layer thickness is better for dimension accuracy [112]. If the layer thickness increases, the dimension of accuracy [113]. A thickness of 0.2–0.3 mm is optimum for accuracy.

Initially, increasing the road width decreases the dimensional accuracy to medium roads width, improving the dimensional accuracy. Changing the raster angle drops the dimensional accuracy. And the negative air gap affects the

Fig. 56 (a) Cylindrical specimen, (b) Accuracy of cylindrical test with different orientation [107]

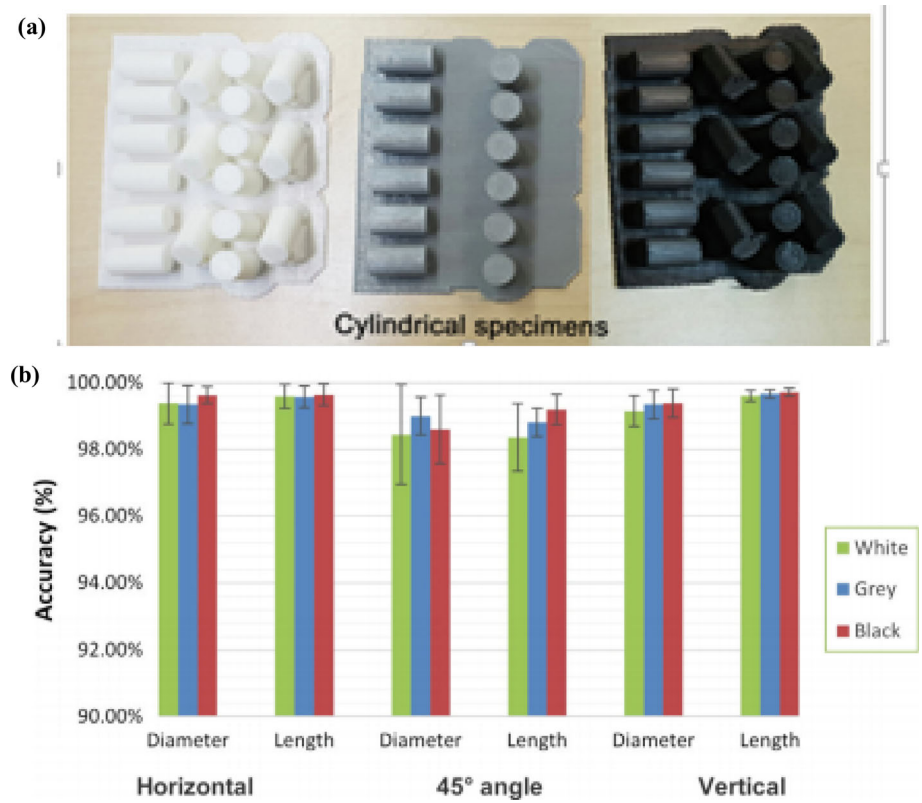


Fig. 57 (a) Dog bone (tensile) specimen, (b) Dog bone test accuracy with various print orientations, raster directions, and layer thicknesses [107]

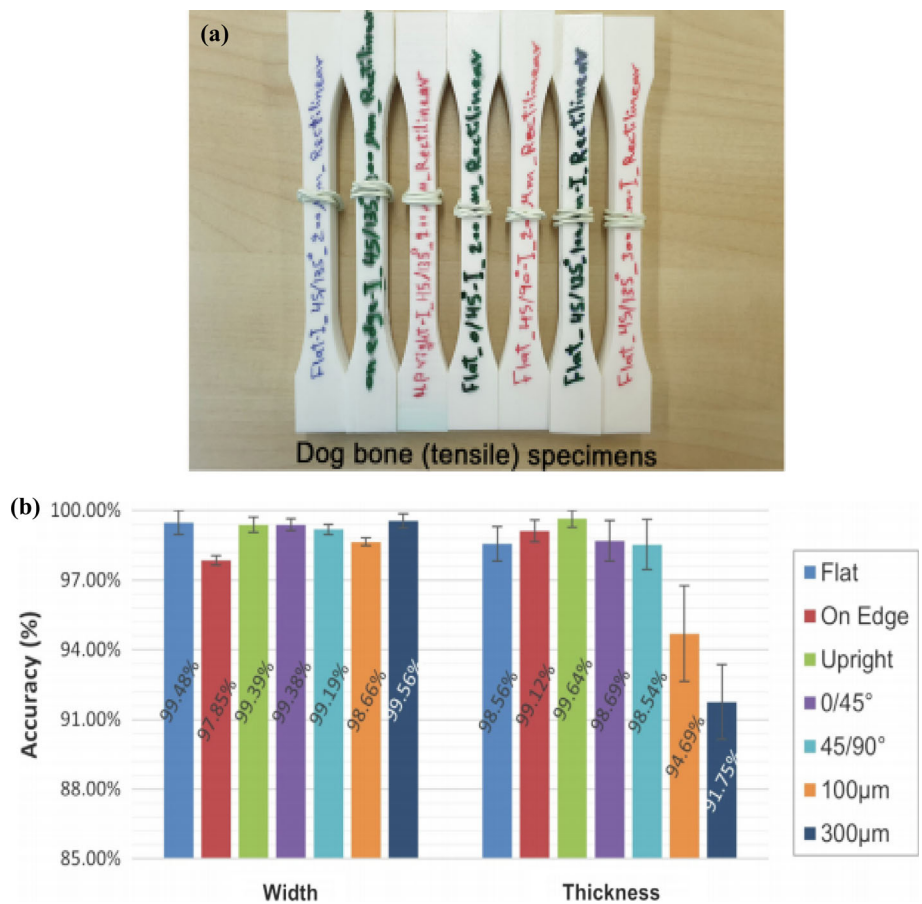


Fig. 58 (a) ME process, (b) Extrusion and Deposition, (c) Coalescence of strand, (d) Cross-sectional morphology, (e) 3D RVE, and (f) Homogenization of RVE [6]

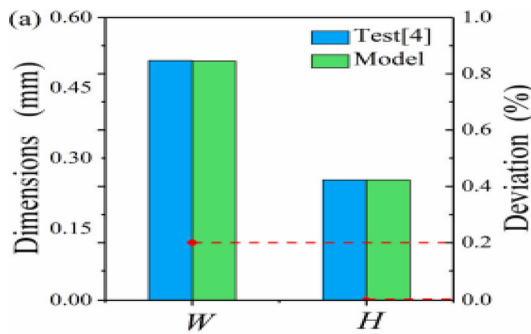
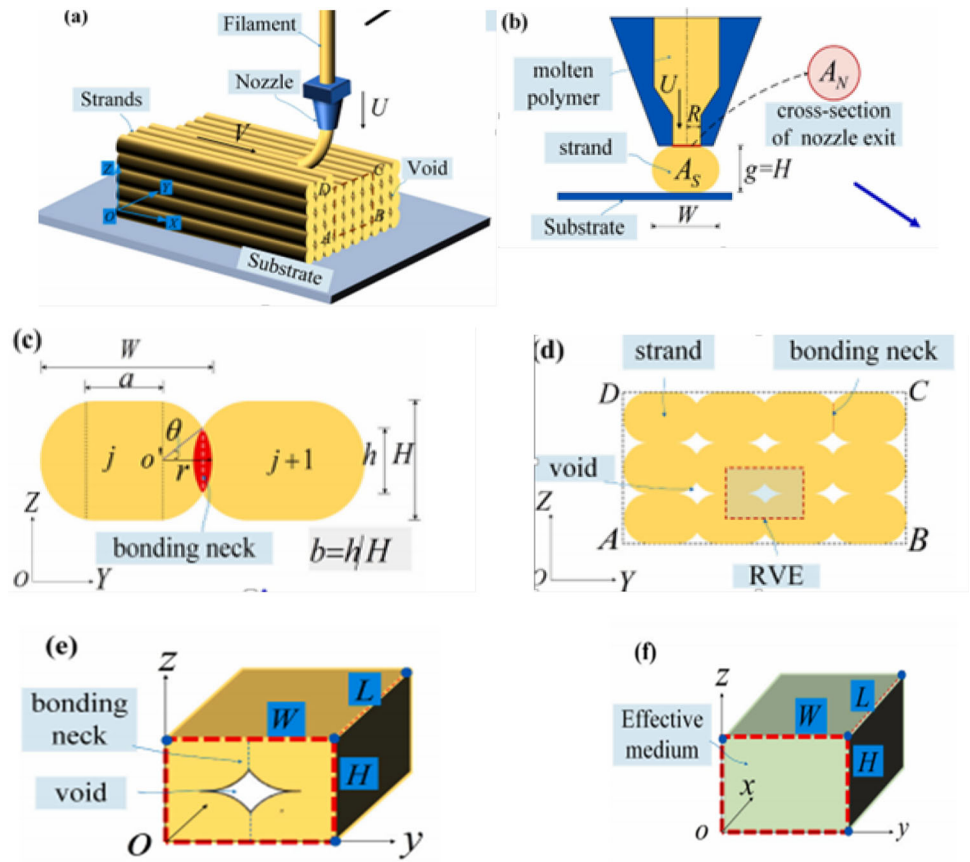


Fig. 59 Dimension vs. W and H [6]

dimensional accuracy [114], and when increasing the air gap is positive to achieve better dimensional accuracy [27].

3 Conclusion

This paper provides details about the fused filaments fabrication (FFF) process parameters, thermal analysis, and their influence on part characteristics. The authors expect that readers will obtain a good knowledge of the FFF process and current research on it. This paper also provides a broad overview of recent research on thermal properties and

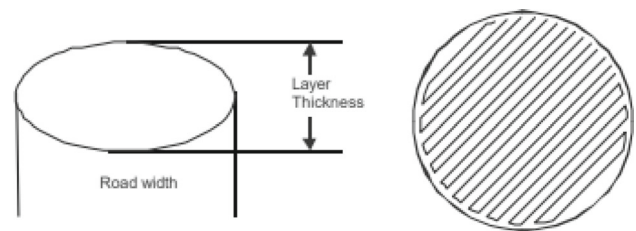


Fig. 60 Raster orientation [27]

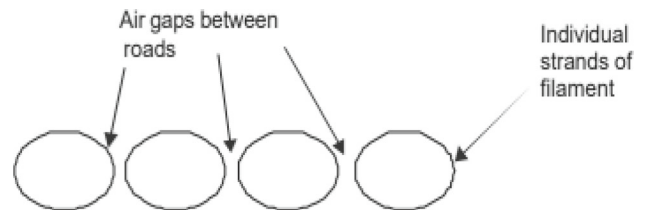
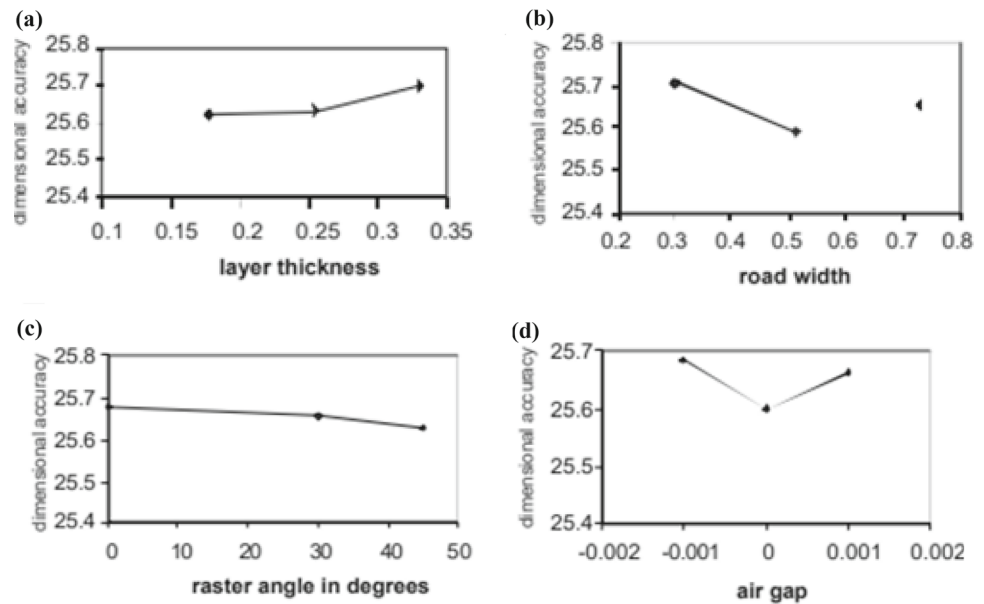


Fig. 61 Air gap between the roads [27]

parameter optimization in the FFF process. Various experimental designs, statistical tools, and optimization approaches have been used. Ultimately, process parameters and thermal properties are considered interconnected and essential for the bond formation, neck growth, and mechanical properties of FFF parts. By adjusting a particular set of thermal

Fig. 62 (a): Dimensional accuracy vs. Layer thickness, (b) Dimensional accuracy vs Road width, (c) Dimensional accuracy vs. Raster angle, and (d) Dimensional accuracy vs. air gap [27]



properties together with process parameters, the quality of printed products, and the performance of the FFF process, will be enhanced. In addition to presenting previous work, the difficulties and scope for future research topics are also discussed. The essential findings from the most recent survey and areas for future research are presented here. The most extensively used materials are presently PLA and ABS. In addition to PLA and ABS, various materials including Nylon, PETG, and composite materials could be used as filament materials for research and manufacture of functional components, enabling a larger spectrum of material possibilities and mechanical characteristics of printed parts. The following conclusion are drawn from the present study:

- The implementation of FFF technology in many industrial applications is currently limited due to faults such as insufficient mechanical characteristics, poor surface quality, and low dimensional accuracy.
- The effects conduction and convection to improve the bond formation and mechanical properties have been investigated.
- Mechanism of neck formation through which study on thermal properties for the improvement in strength, surface finish and dimensional accuracy of printed products. The impact of thermal properties parameters on neck growth includes extrusion temperature, thermal conductivity, diffusivity, heat transfer coefficient, and flow rate.
- The role of bonding between the filaments that affects the parts strength and surface finish of FFF manufactured parts has been investigated by performing thermal properties for neck growth between the filaments. The effect of three input parameters, including nozzle temperature, chamber

temperature, and road gap, on parts strength and surface finish.

- Analysing the influence of bond formation between neighbouring layers that impact the dimensional accuracy of FFF-produced parts has been studied thermal characteristics allowing the construction of neck across the filaments. The role of process parameters such as extrusion temperature and flow rate on the dimensional accuracy of parts.
- The quality of FFF-produced objects is affected by several process parameters, including layer thickness, build orientation, raster width, and print speed.
- Several process parameters, such as the infill pattern, print speed, shell width, and extrusion temperature, are not thoroughly investigated compared to build orientation, raster width, raster orientation, and layer thickness. The fewest relevant process parameters could be used as variables in future research project.
- The FFF procedure is intricate. It comprises multiple steps, each of which has varying degrees of uncertainty. Consider constraints during design and production to increase the quality of printed FFF parts. During the investigation, it is also essential to consider the uncertainty of mathematical methodologies.
- Estimating part properties in the FFF process and combining machine learning techniques and image processing can also be used, emerging in a multidisciplinary research area. Based on previous research findings, various suggestions for future and research gaps have been recognized for the FFF process. The author of this review article expects that by discussing their findings, the average citizen would be inspired to cooperate to overcome the research gaps in the FFF process as well as growing FFF's participation in

a variety of industries and the number of FFF parts on the marketplace.

4 Future scope

The future scope is predicted in additive manufacturing to promote the technology development of a hybrid 3D printer. And 3D printers are efficient in forming products with multi-materials and various colours, improving functional outcomes in bond strength and mechanical, surface finishes, and thermal properties. Optimize the energy. The Decrement of material wastage, modification and recyclable, product accessible, industries, medical, aerospace, automobile, construction, and sciences. Hybrid 3D printers in the future will change the manufacturing industries. A diversity of machine learning and image processing can be employed to predict part qualities in the FDM process, resulting in a multi-disciplinary research area.

Acknowledgements The present work has been funded by the Science and Engineering Research Board- DST under its Start-up Research Grant (SRG) scheme [Grant number: SRG/2019/000943].

References

- Bellehumeur, C., Li, L., Sun, Q., Gu, P.: Modeling of bond formation between polymer filaments in the fused deposition modeling process. *J. Manuf. Process.* **6**, 170–178 (2004). [https://doi.org/10.1016/S1526-6125\(04\)70071-7](https://doi.org/10.1016/S1526-6125(04)70071-7)
- Ravi, A.K., Deshpande, A., Hsu, K.H.: An in-process laser localized pre-deposition heating approach to inter-layer bond strengthening in extrusion based polymer additive manufacturing. *J. Manuf. Process.* **24**, 179–185 (2016). <https://doi.org/10.1016/j.jmapro.2016.08.007>
- Gurralla, P.K., Regalla, S.P.: Part strength evolution with bonding between filaments in fused deposition modelling: this paper studies how coalescence of filaments contributes to the strength of final FDM part. *Virtual Phys. Prototyp.* **9**, 141–149 (2014). <https://doi.org/10.1080/17452759.2014.913400>
- Chacón, J.M., Caminero, M.A., García-Plaza, E., Núñez, P.J.: Additive manufacturing of PLA structures using fused deposition modelling: effect of process parameters on mechanical properties and their optimal selection. *Mater. Des.* **124**, 143–157 (2017). <https://doi.org/10.1016/j.matdes.2017.03.065>
- Turner, B.N., Strong, R., Gold, S.A.: A review of melt extrusion additive manufacturing processes: I. Process design and modeling. *Rapid Prototyp. J.* **20**, 192–204 (2014). <https://doi.org/10.1108/RPJ-01-2013-0012>
- Rao, Y., Wei, N., Yao, S., Wang, K., Peng, Y.: A process-structure-performance modeling for thermoplastic polymers via material extrusion additive manufacturing. *Addit. Manuf.* **39**, 101857 (2021). <https://doi.org/10.1016/j.addma.2021.101857>
- Krishnanand, S., Soni, S., Nayak, A., Taufik, M.: Generation of tool path in fused filament fabrication. In: *Lect. Notes Mech. Eng.*, Springer Science and Business Media Deutschland GmbH, 2021: pp. 153–161. https://doi.org/10.1007/978-981-16-3033-0_14
- Kishore, V., Ajinjeru, C., Nycz, A., Post, B., Lindahl, J., Kunc, V., Duty, C.: Infrared preheating to improve interlayer strength of big area additive manufacturing (BAAM) components. *Addit. Manuf.* **14**, 7–12 (2017). <https://doi.org/10.1016/j.addma.2016.11.008>
- Tamburrino, F., Barone, S., Paoli, A., Razionale, A.V.: Post-processing treatments to enhance additively manufactured polymeric parts: a review. *Virtual Phys. Prototyp.* **16**, 218–251 (2021). <https://doi.org/10.1080/17452759.2021.1917039>
- Lavecchia, F., Guerra, M.G., Galantucci, L.M.: Chemical vapor treatment to improve surface finish of 3D printed polylactic acid (PLA) parts realized by fused filament fabrication. *Prog. Addit. Manuf.* **7**, 65–75 (2022). <https://doi.org/10.1007/s40964-021-00213-2>
- Vaezi, M., Yang, S.: Extrusion-based additive manufacturing of PEEK for biomedical applications. *Virtual Phys. Prototyp.* **10**, 123–135 (2015). <https://doi.org/10.1080/17452759.2015.1097053>
- Ngo, T.D., Kashani, A., Imbalzano, G., Nguyen, K.T.Q., Hui, D.: Additive manufacturing (3D printing): a review of materials, methods, applications and challenges. *Compos. Part B Eng.* **143**, 172–196 (2018). <https://doi.org/10.1016/j.compositesb.2018.02.012>
- Podroužek, J., Marcon, M., Ninčević, K., Wan-Wendner, R.: Bio-inspired 3D infill patterns for additive manufacturing and structural applications. *Materials (Basel)*. **12**, 499 (2019). <https://doi.org/10.3390/ma12030499>
- Cholleti, E.R., Gibson, I.: ABS nano composite materials in additive manufacturing. *IOP Conf. Ser. Mater. Sci. Eng.* (2018). <https://doi.org/10.1088/1757-899X/455/1/012038>
- Serdeczny, M.P., Comminal, R., Pedersen, D.B., Spangenberg, J.: Numerical simulations of the mesostructure formation in material extrusion additive manufacturing. *Addit. Manuf.* **28**, 419–429 (2019). <https://doi.org/10.1016/j.addma.2019.05.024>
- Kim, M.K., Lee, I.H., Kim, H.C.: Effect of fabrication parameters on surface roughness of FDM parts. *Int. J. Precis. Eng. Manuf.* **19**, 137–142 (2018). <https://doi.org/10.1007/s12541-018-0016-0>
- Sun, Q., Rizvi, G.M., Bellehumeur, C.T., Gu, P.: Effect of processing conditions on the bonding quality of FDM polymer filaments. *Rapid Prototyp. J.* **14**, 72–80 (2008). <https://doi.org/10.1108/13552540810862028>
- Li, L., Sun, Q., Bellehumeur, C., Gu, P.: Investigation of bond formation in FDM process investigation of bond formation in FDM process. *Trans. North Am. Manuf. Res. Inst. SME*. **31**, 400–407 (2019)
- Bhalodi, D.V., Zalavadiya, K.S., Gurralla, P.K.: Parametric study to predict the bond formation in FDM process. *Int. J. Mater. Mech. Manuf.* **6**, 313–316 (2018)
- Syrlybayev, D., Zharylkassyn, B., Seisekulova, A., Akhmetov, M., Perveen, A., Talamona, D.: Optimisation of strength properties of FDM printed parts—a critical review. *Polymers (Basel)*. **13**, 1587 (2021). <https://doi.org/10.3390/polym13101587>
- Dey, A., Yodo, N.: A systematic survey of FDM process parameter optimization and their influence on part characteristics. *J. Manuf. Mater. Process.* **3**, 64 (2019). <https://doi.org/10.3390/jmmp3030064>
- Garzon-Hernandez, S., Garcia-Gonzalez, D., Jérusalem, A., Arias, A.: Design of FDM 3D printed polymers: an experimental-modelling methodology for the prediction of mechanical properties. *Mater. Des.* **188**, 108414 (2020). <https://doi.org/10.1016/j.matdes.2019.108414>
- Conley, W.H., Deferrari, R.J.: Principles and applications. *J. Higher Educ.* **23**, 225 (1952). <https://doi.org/10.2307/1976787>
- Rodríguez, J.F., Thomas, J.P., Renaud, J.E.: Mechanical behavior of acrylonitrile butadiene styrene (ABS) fused deposition materials. Experimental investigation. *Rapid Prototyp. J.* **7**, 148–158 (2001). <https://doi.org/10.1108/13552540110395547>
- Dhinesh, S.K., Arun Prakash, S., Senthil Kumar, K.L., Megalingam, A.: Study on flexural and tensile behavior of PLA,

- ABS and PLA-ABS materials. *Mater. Today Proc.* (2021). <https://doi.org/10.1016/j.matpr.2020.03.546>
26. Wang, P., Zou, B., Ding, S.: Modeling of surface roughness based on heat transfer considering diffusion among deposition filaments for FDM 3D printing heat-resistant resin. *Appl. Therm. Eng.* **161**, 114064 (2019). <https://doi.org/10.1016/j.applthermaleng.2019.114064>
 27. Raju, T.N., Ramach, V., Raju, R.: An experimental investigation on surface quality and dimensional accuracy of FDM components, (n.d.). <http://citeseerx.ist.psu.edu/viewdoc/summary?doi=10.1.1.670.108> (accessed May 26, 2022).
 28. Popescu, D., Zapciu, A., Amza, C., Baci, F., Marinescu, R.: FDM process parameters influence over the mechanical properties of polymer specimens: a review. *Polym. Test.* **69**, 157–166 (2018). <https://doi.org/10.1016/j.polymertesting.2018.05.020>
 29. Yin, J., Lu, C., Fu, J., Huang, Y., Zheng, Y.: Interfacial bonding during multi-material fused deposition modeling (FDM) process due to inter-molecular diffusion. *Mater. Des.* **150**, 104–112 (2018). <https://doi.org/10.1016/j.matdes.2018.04.029>
 30. Ouballouch, A., Lasri, L., Ouahmane, I., El Alaiji, R., Sallaou, M., Ettaqi, S.: Optimization of PLA parts manufactured by the Fused Deposition Modeling Technology. In: 2018 IEEE Int. Conf. Technol. Manag. Oper. Decis. ICTMOD 2018, Institute of Electrical and Electronics Engineers Inc., 2018;288–292. <https://doi.org/10.1109/ITMC.2018.8691133>
 31. Jain, P.K., Pandey, P.M., Rao, P.V.M.: Experimental investigations for improving part strength in selective laser sintering. *Virtual Phys. Prototyp.* **3**, 177–188 (2008). <https://doi.org/10.1080/17452750802065893>
 32. Tao, Y., Wang, H., Li, Z., Li, P., Shi, S.Q.: Development and application of wood flour-filled polylactic acid composite filament for 3d printing. *Materials (Basel)* (2017). <https://doi.org/10.3390/ma10040339>
 33. Vanaei, H., Shirinbayan, M., Deligant, M., Raissi, K., Fitoussi, J., Khelladi, S., Tcharkhtchi, A.: Influence of process parameters on thermal and mechanical properties of polylactic acid fabricated by fused filament fabrication. *Polym. Eng. Sci.* **60**, 1822–1831 (2020). <https://doi.org/10.1002/pen.25419>
 34. Kuznetsov, V., Solonin, A., Urzhumtsev, O., Schilling, R., Tavittov, A.: Strength of PLA components fabricated with fused deposition technology using a desktop 3D printer as a function of geometrical parameters of the process. *Polymers (Basel)*. **10**, 313 (2018). <https://doi.org/10.3390/polym10030313>
 35. Rodríguez-Panes, A., Claver, J., Camacho, A.: The influence of manufacturing parameters on the mechanical behaviour of PLA and ABS pieces manufactured by FDM: a comparative analysis. *Materials (Basel)*. **11**, 1333 (2018). <https://doi.org/10.3390/ma11081333>
 36. Aloyaydi, B., Sivasankaran, S., Mustafa, A.: Investigation of infill-patterns on mechanical response of 3D printed poly-lactic-acid. *Polym. Test.* **87**, 106557 (2020). <https://doi.org/10.1016/j.polymertesting.2020.106557>
 37. Poly(lactic Acid): PLA Biopolymer Technology and Applications | Request PDF, (n.d.). [https://www.researchgate.net/publication/286177523_Poly\(lactic_Acid\)_PLA_Biopolymer_Technology_and_Applications](https://www.researchgate.net/publication/286177523_Poly(lactic_Acid)_PLA_Biopolymer_Technology_and_Applications) (accessed May 20, 2022)
 38. Yan, Y., Zhang, R., Hong, G., Yuan, X.: Research on the bonding of material paths in melted extrusion modeling. *Mater. Des.* **21**, 93–99 (2000). [https://doi.org/10.1016/s0261-3069\(99\)00058-8](https://doi.org/10.1016/s0261-3069(99)00058-8)
 39. Triyono, J., Sukanto, H., Saputra, R.M., Smaradhana, D.F.: The effect of nozzle hole diameter of 3D printing on porosity and tensile strength parts using polylactic acid material. *Open Eng.* **10**, 762–768 (2020). <https://doi.org/10.1515/eng-2020-0083>
 40. Chua, B.-L., Baek, S.-H., Park, K., Ahn, D.-G.: Numerical investigation of deposition characteristics of PLA on an ABS plate using a material extrusion process. *Materials (Basel)*. **14**, 3404 (2021). <https://doi.org/10.3390/ma14123404>
 41. Abeykoon, C., Sri-Amphorn, P., Fernando, A.: Optimization of fused deposition modeling parameters for improved PLA and ABS 3D printed structures. *Int. J. Light. Mater. Manuf.* **3**, 284–297 (2020). <https://doi.org/10.1016/j.ijlmm.2020.03.003>
 42. Partain, S.C.: Fused deposition modeling with localized pre-deposition heating using forced air, Montana State University - Bozeman, College of Engineering, 2007. <https://scholarworks.montana.edu/xmlui/bitstream/1/2016/1/PartainS0507.pdf> (accessed May 26, 2022)
 43. Bellini, A., Güçeri, S.: Mechanical characterization of parts fabricated using fused deposition modeling. *Rapid Prototyp. J.* **9**, 252–264 (2003). <https://doi.org/10.1108/13552540310489631>
 44. Yardimci, M.A., Güçeri, S.: Conceptual framework for the thermal process modelling of fused deposition. *Rapid Prototyp. J.* **2**, 26–31 (1996). <https://doi.org/10.1108/13552549610128206>
 45. Zmeskal, O., Marackova, L., Lapcikova, T., Mencik, P., Prikrýl, R.: Thermal properties of samples prepared from polylactic acid by 3D printing, in: AIP Conf. Proc., American Institute of Physics Inc., 2020;020022. <https://doi.org/10.1063/5.0033857>
 46. Jiang, K.Y., Gu, Y.H.: Controlling parameters for polymer melting and extrusion in FDM. *Key Eng. Mater.* (2004). <https://doi.org/10.4028/www.scientific.net/kem.259-260.667>
 47. Vollmer, M., Möllmann, K.-P.: Some basic concepts of heat transfer. 2010. <https://doi.org/10.1002/9783527630868.ch4>
 48. Pokluda, O., Bellehumeur, C.T., Vlachopoulos, J.: Modification of Frenkel's model for sintering. *AIChE J.* **43**, 3253–3256 (1997). <https://doi.org/10.1002/aic.690431213>
 49. Sood, A.K., Ohdar, R.K., Mahapatra, S.S.: Parametric appraisal of mechanical property of fused deposition modelling processed parts. *Mater. Des.* **31**, 287–295 (2010). <https://doi.org/10.1016/j.matdes.2009.06.016>
 50. Nickel, A.H., Barnett, D.M., Prinz, F.B.: Thermal stresses and deposition patterns in layered manufacturing. *Mater. Sci. Eng. A.* **317**, 59–64 (2001). [https://doi.org/10.1016/S0921-5093\(01\)01179-0](https://doi.org/10.1016/S0921-5093(01)01179-0)
 51. Anitha, R., Arunachalam, S., Radhakrishnan, P.: Critical parameters influencing the quality of prototypes in fused deposition modelling. *J. Mater. Process. Technol.* (2001). [https://doi.org/10.1016/S0924-0136\(01\)00980-3](https://doi.org/10.1016/S0924-0136(01)00980-3)
 52. Coogan, T.J., Kazmer, D.O.: Bond and part strength in fused deposition modeling. *Rapid Prototyp. J.* **23**, 414–422 (2017). <https://doi.org/10.1108/RPJ-03-2016-0050>
 53. Shofner, M.L., Lozano, K., Rodríguez-Macías, F.J., Barrera, E.V.: Nanofiber-reinforced polymers prepared by fused deposition modeling. *J. Appl. Polym. Sci.* **89**, 3081–3090 (2003). <https://doi.org/10.1002/app.12496>
 54. Sezer, H.K., Eren, O.: FDM 3D printing of MWCNT re-inforced ABS nano-composite parts with enhanced mechanical and electrical properties. *J. Manuf. Process.* **37**, 339–347 (2019). <https://doi.org/10.1016/j.jmapro.2018.12.004>
 55. Dul, S., Fambri, L., Pegoretti, A.: Filaments production and fused deposition modelling of ABS/carbon nanotubes composites. *Nanomaterials* (2018). <https://doi.org/10.3390/nano8010049>
 56. Bardot, M., Schulz, M.D.: Biodegradable Poly(Lactic Acid) nanocomposites for fused deposition modeling 3D printing. *Nanomaterials* **10**, 2567 (2020). <https://doi.org/10.3390/nano10122567>
 57. Coppola, B., Cappetti, N., Di Maio, L., Scarfato, P., Incarnato, L.: 3D printing of PLA/clay nanocomposites: influence of printing temperature on printed samples properties. *Materials (Basel)*. **11**, 1947 (2018). <https://doi.org/10.3390/ma11101947>
 58. Qiu, D., Langrana, N.A.: Void eliminating toolpath for extrusion-based multi-material layered manufacturing. *Rapid Prototyp. J.* **8**, 38–45 (2002). <https://doi.org/10.1108/13552540210413293>

59. Mamaghani Shishavan, S., Azdast, T., Rash Ahmadi, S.: Investigation of the effect of nanoclay and processing parameters on the tensile strength and hardness of injection molded Acrylonitrile Butadiene Styrene-organoclay nanocomposites. *Mater. Des.* **58**, 527–534 (2014). <https://doi.org/10.1016/j.matdes.2014.02.014>
60. Pavlidou, S., Papispyrides, C.D.: A review on polymer-layered silicate nanocomposites. *Prog. Polym. Sci.* **33**, 1119–1198 (2008). <https://doi.org/10.1016/j.progpolymsci.2008.07.008>
61. Francis, V., Jain, P.K.: Experimental investigations on fused deposition modelling of polymer-layered silicate nanocomposite. *Virtual Phys. Prototyp.* **11**, 109–121 (2016). <https://doi.org/10.1080/17452759.2016.1172431>
62. Rajpurohit, S.R., Dave, H.K.: Effect of process parameters on tensile strength of FDM printed PLA part. *Rapid Prototyp. J.* **24**, 1317–1324 (2018). <https://doi.org/10.1108/RPJ-06-2017-0134>
63. Hernandez, R., Slaughter, D., Whaley, D., Tate, J., Asiabanpour, B., Analyzing the tensile, compressive, and flexural properties of 3D printed ABS P430 plastic based on printing orientation using fused deposition modeling, *Solid Free. Fabr. 2016 Proc. 27th Annu. Int. Solid Free. Fabr. Symp. - An Addit. Manuf. Conf. SFF 2016*. 2016;939–950
64. Ziemian, S., Okwara, M., Ziemian, C.W.: Tensile and fatigue behavior of layered acrylonitrile butadiene styrene. *Rapid Prototyp. J.* **21**, 270–278 (2015). <https://doi.org/10.1108/RPJ-09-2013-0086>
65. Jain, P.K., Pandey, P.M., Rao, P.V.M.: Effect of delay time on part strength in selective laser sintering. *Int. J. Adv. Manuf. Technol.* **43**, 117–126 (2009). <https://doi.org/10.1007/S00170-008-1682-3>
66. Garg, A., Bhattacharya, A.: An insight to the failure of FDM parts under tensile loading: finite element analysis and experimental study. *Int. J. Mech. Sci.* **120**, 225–236 (2017). <https://doi.org/10.1016/j.ijmecsci.2016.11.032>
67. Aliheidari, N., Tripuraneni, R., Ameli, A., Nadimpalli, S.: Fracture resistance measurement of fused deposition modeling 3D printed polymers. *Polym. Test.* **60**, 94–101 (2017). <https://doi.org/10.1016/j.polymertesting.2017.03.016>
68. (PDF) Prediction of neck growth due to inter and intra-layer bonding for high strength parts in additive manufacturing, (n.d.). https://www.researchgate.net/publication/264545454_Prediction_of_Neck_Growth_due_to_Inter_and_Intra-Layer_Bonding_for_High_Strength_Parts_in_Additive_Manufacturing (accessed May 20, 2022)
69. Chadha, A., Ul Haq, M.I., Raina, A., Singh, R.R., Penumarti, N.B., Bishnoi, M.S.: Effect of fused deposition modelling process parameters on mechanical properties of 3D printed parts. *World J. Eng.* **16**, 550–559 (2019). <https://doi.org/10.1108/WJE-09-2018-0329>
70. Ćwikła, G., Grabowik, C., Kalinowski, K., Paprocka, I., Ociepa, P.: The influence of printing parameters on selected mechanical properties of FDM/FFF 3D-printed parts. In: *IOP Conf. Ser. Mater. Sci. Eng.*, Institute of Physics Publishing, 2017;012033. <https://doi.org/10.1088/1757-899X/227/1/012033>
71. Kulkarni, P., Dutta, D.: Deposition strategies and resulting part stiffnesses in fused deposition modeling. *J. Manuf. Sci. Eng. Trans. ASME.* **121**, 93–103 (1999). <https://doi.org/10.1115/1.2830582>
72. Ang, K.C., Leong, K.F., Chua, C.K., Chandrasekaran, M.: Investigation of the mechanical properties and porosity relationships in fused deposition modelling-fabricated porous structures. *Rapid Prototyp. J.* **12**, 100–105 (2006). <https://doi.org/10.1108/13552540610652447>
73. Zhang, Y., Chou, K.: A parametric study of part distortions in fused deposition modelling using three-dimensional finite element analysis. *Proc. Inst. Mech. Eng. Part B J. Eng. Manuf.* **222**, 959–968 (2008). <https://doi.org/10.1243/09544054JEM990>
74. Radhwan, H., Shayfull, Z., Abdellah, A.E.H., Irfan, A.R., Kamarudin, K.: Optimization parameter effects on the strength of 3D-printing process using Taguchi method. In: *AIP Conf. Proc.*, American Institute of Physics Inc., 2019;020154. <https://doi.org/10.1063/1.5118162>
75. Vicente, C.M.S., Martins, T.S., Leite, M., Ribeiro, A., Reis, L.: Influence of fused deposition modeling parameters on the mechanical properties of ABS parts. *Polym. Adv. Technol.* **31**, 501–507 (2020). <https://doi.org/10.1002/pat.4787>
76. Crococo, D., De Agostinis, M., Olmi, G.: Experimental characterization and analytical modelling of the mechanical behaviour of fused deposition processed parts made of ABS-M30. *Comput. Mater. Sci.* **79**, 506–518 (2013). <https://doi.org/10.1016/j.commatsci.2013.06.041>
77. Reddy, B.V., Reddy, N.V., Ghosh, A.: Fused deposition modelling using direct extrusion. *Virtual Phys. Prototyp.* **2**, 51–60 (2007). <https://doi.org/10.1080/17452750701336486>
78. A Visual Tool to Improve Layered Manufacturing Part Quality, (n.d.). <https://repositories.lib.utexas.edu/handle/2152/73466> (accessed May 26, 2022)
79. Sahu, R.K., Mahapatra, S.S., Sood, A.K.: A study on dimensional accuracy of fused deposition modeling (FDM) processed parts using fuzzy logic. *J. Manuf. Sci. Prod.* **13**, 183–197 (2014). <https://doi.org/10.1515/jmsp-2013-0010>
80. Bhalodi, D., Zalavadiya, K., Gurralla, P.K.: Influence of temperature on polymer parts manufactured by fused deposition modeling process. *J. Brazilian Soc. Mech. Sci. Eng.* **41**, 1–11 (2019). <https://doi.org/10.1007/s40430-019-1616-z>
81. Akande, S.O.: Dimensional accuracy and surface finish optimization of fused deposition modelling parts using desirability function analysis. *Int. J. Eng. Res.* (2015). <https://doi.org/10.17577/ijertv4is040393>
82. Wang, T.M., Xi, J.T., Jin, Y.: A model research for prototype warp deformation in the FDM process. *Int. J. Adv. Manuf. Technol.* **33**, 1087–1096 (2007). <https://doi.org/10.1007/s00170-006-0556-9>
83. Xiaoyong, S., Liangcheng, C., Honglin, M., Peng, G., Zhanwei, B., Cheng, L.: Experimental analysis of high temperature PEEK materials on 3D printing test. In: *Proc. - 9th Int. Conf. Meas. Technol. Mechatronics Autom. ICMTMA 2017*, Institute of Electrical and Electronics Engineers Inc., 2017; 13–16. <https://doi.org/10.1109/ICMTMA.2017.0012>
84. Tardif, X., Pignon, B., Boyard, N., Schmelzer, J.W.P., Sobotka, V., Delaunay, D., Schick, C.: Experimental study of crystallization of PolyEtherEtherKetone (PEEK) over a large temperature range using a nano-calorimeter. *Polym. Test.* **36**, 10–19 (2014). <https://doi.org/10.1016/j.polymertesting.2014.03.013>
85. Wu, W.Z., Geng, P., Zhao, J., Zhang, Y., Rosen, D.W., Zhang, H.B.: Manufacture and thermal deformation analysis of semicrystalline polymer polyether ether ketone by 3D printing. *Mater. Res. Innov.* **18**, S5-12-S5-16 (2014). <https://doi.org/10.1179/1432891714Z.000000000898>
86. Durgun, I., Ertan, R.: Experimental investigation of FDM process for improvement of mechanical properties and production cost. *Rapid Prototyp. J.* **20**, 228–235 (2014). <https://doi.org/10.1108/RPJ-10-2012-0091>
87. Jatti, V.S., Jatti, S.V., Patel, A.P., Jatti, V.S.: A study on effect of fused deposition modeling process parameters on mechanical properties. *Int. J. Sci. Technol. Res.* **8**, 689–693 (2019)
88. Garg, A., Bhattacharya, A., Batish, A.: Chemical vapor treatment of ABS parts built by FDM: analysis of surface finish and mechanical strength. *Int. J. Adv. Manuf. Technol.* **89**, 2175–2191 (2017). <https://doi.org/10.1007/s00170-016-9257-1>
89. Francis, V., Jain, P.K.: Investigation on the effect of surface modification of 3D printed parts by nanoclay and dimethyl ketone, <https://doi.org/10.1080/>

- 10426914.2017.1401717. 2017;33:1080–1092. <https://doi.org/10.1080/10426914.2017.1401717>
90. Frone, A.N., Batalu, D., Chiulan, I., Oprea, M., Gabor, A.R., Nicolae, C.-A., Raditoiu, V., Trusca, R., Panaitescu, D.M.: Morpho-structural, thermal and mechanical properties of PLA/PHB/cellulose biodegradable nanocomposites obtained by compression molding, extrusion, and 3D printing. *Nanomaterials* **10**, 51 (2019). <https://doi.org/10.3390/nano10010051>
 91. Suh, C.H., Jung, Y.C., Kim, Y.S.: Effects of thickness and surface roughness on mechanical properties of aluminum sheets. *J. Mech. Sci. Technol.* **24**, 2091–2098 (2010). <https://doi.org/10.1007/s12206-010-0707-7>
 92. Ahn, D., Kweon, J.H., Kwon, S., Song, J., Lee, S.: Representation of surface roughness in fused deposition modeling. *J. Mater. Process. Technol.* **209**, 5593–5600 (2009). <https://doi.org/10.1016/j.jmatprotec.2009.05.016>
 93. Vasudevarao, B., Natarajan, D.P., Henderson, M.: Sensitivity of Rp surface finish to process. *Solid Free. Fabr. Proc.* 2000;251–258. http://prism.asu.edu/publications/papers/paper00_srpsfppv.pdf
 94. Ahn, D., Kim, H., Lee, S.: Surface roughness prediction using measured data and interpolation in layered manufacturing. *J. Mater. Process. Technol.* **209**, 664–671 (2009). <https://doi.org/10.1016/j.jmatprotec.2008.02.050>
 95. Es-Said, O.S., Foyos, J., Noorani, R., Mendelson, M., Marloth, R., Pregger, B.A.: Effect of layer orientation on mechanical properties of rapid prototyped samples. *Mater. Manuf. Process.* **15**, 107–122 (2000). <https://doi.org/10.1080/10426910008912976>
 96. Taufik, M., Jain, P.K.: Role of build orientation in layered manufacturing: a review. *Int. J. Manuf. Technol. Manag.* **27**, 47–73 (2013). <https://doi.org/10.1504/IJMTM.2013.058637>
 97. Chennakesava, P. and Shivraj Narayan, Y.: Fused deposition modeling – insights. *Int. Conf. Adv. Des. Manuf.* 2014;1345–1350. https://www.researchgate.net/publication/269702639_Fused_Deposition_Modeling_-_Insights (accessed May 26, 2022).
 98. Boschetto, A., Giordano, V., Veniali, F.: 3D roughness profile model in fused deposition modelling. *Rapid Prototyp. J.* **19**, 240–252 (2013). <https://doi.org/10.1108/13552541311323254>
 99. Ippolito, R., Iuliano, L., Gatto, A.: Benchmarking of rapid prototyping techniques in terms of dimensional accuracy and surface finish. *CIRP Ann. - Manuf. Technol.* **44**, 157–160 (1995). [https://doi.org/10.1016/S0007-8506\(07\)62296-3](https://doi.org/10.1016/S0007-8506(07)62296-3)
 100. Gadelmawla, E.S., Koura, M.M., Maksoud, T.M.A., Elewa, I.M., Soliman, H.H.: Roughness parameters. *J. Mater. Process. Technol.* **123**, 133–145 (2002). [https://doi.org/10.1016/S0924-0136\(02\)00060-2](https://doi.org/10.1016/S0924-0136(02)00060-2)
 101. Galantucci, L.M., Lavecchia, F., Percoco, G.: Experimental study aiming to enhance the surface finish of fused deposition modeled parts. *CIRP Ann. - Manuf. Technol.* **58**, 189–192 (2009). <https://doi.org/10.1016/j.cirp.2009.03.071>
 102. Huang, B., Singamneni, S.: Raster angle mechanics in fused deposition modelling. *J. Compos. Mater.* **49**, 363–383 (2015). <https://doi.org/10.1177/0021998313519153>
 103. Górski, F., Kuczko, W., Wichniarek, R.: Influence of process parameters on dimensional accuracy of parts manufactured using fused deposition modelling technology. *Adv. Sci. Technol. Res. J.* **7**, 27–35 (2013). <https://doi.org/10.5604/20804075.1062340>
 104. Alafaghani, A., Qattawi, A., Alrawi, B., Guzman, A.: Experimental optimization of fused deposition modelling processing parameters: a design-for-manufacturing approach. In: *Procedia Manuf.*, Elsevier B.V., 2017;791–803. <https://doi.org/10.1016/j.promfg.2017.07.079>
 105. Akhoundi, B., Behraves, A.H.: Effect of filling pattern on the tensile and flexural mechanical properties of FDM 3D printed products. *Exp. Mech.* **59**, 883–897 (2019). <https://doi.org/10.1007/s11340-018-00467-y>
 106. Luis Pérez, C.J.: Analysis of the surface roughness and dimensional accuracy capability of fused deposition modelling processes. *Int. J. Prod. Res.* **40**, 2865–2881 (2002). <https://doi.org/10.1080/00207540210146099>
 107. Hanon, M.M., Zsidai, L., Ma, Q.: Accuracy investigation of 3D printed PLA with various process parameters and different colors. *Mater. Today Proc.* (2021). <https://doi.org/10.1016/j.matpr.2020.12.1246>
 108. Beniak, J., Križan, P., Šooš, L., Matuš, M.: Research on shape and dimensional accuracy of FDM produced parts. In: *IOP Conf. Ser. Mater. Sci. Eng.*, Institute of Physics Publishing, 2019; 012030. <https://doi.org/10.1088/1757-899X/501/1/012030>
 109. Wang, C.C., Lin, T.W., Hu, S.S.: Optimizing the rapid prototyping process by integrating the Taguchi method with the Gray relational analysis. *Rapid Prototyp. J.* **13**, 304–315 (2007). <https://doi.org/10.1108/13552540710824814>
 110. Nidagundi, V.B., Keshavamurthy, R., Prakash, C.P.S.: Studies on parametric optimization for fused deposition modelling process. *Mater. Today Proc.* (2015). <https://doi.org/10.1016/j.matpr.2015.07.097>
 111. Bähr, F., Westkämper, E.: Correlations between influencing parameters and quality properties of components produced by fused deposition modeling. *Procedia CIRP* (2018). <https://doi.org/10.1016/j.procir.2018.03.048>
 112. D'Amico, A.A., Debaie, A., Peterson, A.M.: Effect of layer thickness on irreversible thermal expansion and interlayer strength in fused deposition modeling. *Rapid Prototyp. J.* **23**, 943–953 (2017). <https://doi.org/10.1108/RPJ-05-2016-0077>
 113. Zhou, J.G., Herscovici, D., Chen, C.C.: Parametric process optimization to improve the accuracy of rapid prototyped stereolithography parts. *Int. J. Mach. Tools Manuf.* **40**, 363–379 (2000). [https://doi.org/10.1016/S0890-6955\(99\)00068-1](https://doi.org/10.1016/S0890-6955(99)00068-1)
 114. Raghunath, N., Pandey, P.M.: Improving accuracy through shrinkage modelling by using Taguchi method in selective laser sintering. *Int. J. Mach. Tools Manuf.* **47**, 985–995 (2007). <https://doi.org/10.1016/j.ijmachtools.2006.07.001>